REAL-TIME SIMULATION OF SOIL–TOOL INTERACTION USING ADVANCED SOIL MODELS

A THESIS SUBMITTED TO
THE GRADUATE SCHOOL OF NATURAL AND APPLIED SCIENCES
OF
MIDDLE EAST TECHNICAL UNIVERSITY

BY

MÜCAHIT GÜRBÜZ

IN PARTIAL FULFILLMENT OF THE REQUIREMENTS
FOR
THE DEGREE OF MASTER OF SCIENCE
IN
CIVIL ENGINEERING

SEPTEMBER 2019

Approval of the thesis:

REAL-TIME SIMULATION OF SOIL–TOOL INTERACTION USING ADVANCED SOIL MODELS

submitted by **MÜCAHIT GÜRBÜZ** in partial fulfillment of the requirements for the degree of **Master of Science in Civil Engineering Department, Middle East Technical University** by,

Prof. Dr. Halil Kalıpçılar
Dean, Graduate School of **Natural and Applied Sciences**

Prof. Dr. Ahmet Türer
Head of Department, **Civil Engineering**

Assist. Prof. Dr. Onur Pekcan
Supervisor, **Civil Engineering, METU**

Examining Committee Members:

Assoc. Prof. Dr. Zeynep Gülerce
Civil Engineering, METU

Assist. Prof. Dr. Onur Pekcan
Civil Engineering, METU

Prof. Dr. Erdal Çokca
Civil Engineering, METU

Assist. Prof. Dr. Nabi Kartal Toker
Civil Engineering, METU

Assist. Prof. Dr. Sevinç Ünsal Oral
Civil Engineering, Başkent University

Date: 09.09.2019

I hereby declare that all information in this document has been obtained and presented in accordance with academic rules and ethical conduct. I also declare that, as required by these rules and conduct, I have fully cited and referenced all material and results that are not original to this work.

Name, Surname: Mücahit Gürbüz

Signature:

ABSTRACT

REAL-TIME SIMULATION OF SOIL–TOOL INTERACTION USING ADVANCED SOIL MODELS

Gürbüz, Mücahit
Master of Science, Civil Engineering
Supervisor: Assist. Prof. Dr. Onur Pekcan

September 2019, 97 pages

Excavation work is one of the main elements needed in construction fields. To meet such a huge demand, a large number of excavators are working all over the globe. In addition, researchers and companies put enormous efforts to develop more efficient excavator models. With the advancement of technology, autonomous systems have become popular and ideal way to upgrade machines for faster, cheaper and safer production. Not surprisingly, there have been many attempts to develop fully autonomous robotic excavation systems and this has become one of the trending topics in the earth-moving industry. There are some key challenges in developing an autonomous excavation system. For example, accurate and fast prediction of resisting soil forces on the excavator bucket plays a crucial role in developing unmanned excavator systems. Current studies provide unrealistic and/or computationally expensive soil-tool interaction models. This study represents a new method to solve the interaction of excavator bucket and soil in real-time with acceptable accuracy. Through the developed accurate real-time soil-tool interaction simulation, it is also aimed to make further progress in virtual reality systems requiring real-time simulations, cabin simulators, and computer games.

Keywords: Excavator Simulation, Soil-tool Interaction, Unsaturated Soils, Real-time Simulation

ÖZ

İLERİ ZEMİN MEKANİĞİ MODELLERİ KULLANILARAK GERÇEK ZAMANLI ZEMİN-ARAÇ ETKİLEŞİM SİMÜLASYONU GELİŞTİRİLMESİ

Gürbüz, Mücahit
Yüksek Lisans, İnşaat Mühendisliği
Tez Danışmanı: Dr. Öğr. Üyesi Onur Pekcan

Eylül 2019, 97 sayfa

Kazı işleri, inşaat sahalarında en çok ihtiyaç duyulan iş kalemlerinin başında yer almaktadır. Bu ihtiyacı karşılamak üzere, dünyanın her yerinde çok sayıda ekskavatör çalışmaktadır. Bunun yanı sıra araştırmacılar ve şirketler daha etkin ekskavatör sistemleri geliştirme üzerine çalışmalar gerçekleştirmektedir. Gelişen teknolojinin de yardımıyla, otonom ekskavatör sistemleri kazı işlerinde sağladıkları hız, ucuzluk ve güvenlik nedeniyle, ideal ve popüler bir üretim hedefi olmuştur. Şaşırtıcı olmayan bir şekilde tam otonom robotik ekskavatör sistemleri üzerine birçok deneme gerçekleşmiş ve bu denemeler kazı-dolgu sektöründeki en popüler konu başlıkları arasına girmiştir. Bu sistemlerin geliştirilmesi esnasında geliştiricilerin karşılaştıkları bazı zorluklar dikkat çekmektedir; örneğin insansız ekskavatör sistemi geliştirilmesi yönündeki önemli noktalardan birisi, hızlı ve tutarlı bir şekilde zemin tepki kuvvetlerinin tahmin edilmesidir. Güncel çalışmalar gerçekçi olmayan ve/veya yüksek işlem gücü gerektiren zemin-araç etkileşim modelleri sunmaktadır. Bu tez gerçek zamanlı ve kabul edilebilir tutarlılıkta sonuçlar veren yeni bir zemin-ekskavatör kepçesi etkileşim metodu önermektedir. Bu tutarlı ve gerçek zamanlı zemin-araç etkileşim metodu ile otonom ekskavatör sistemlerinin yanı sıra, gerçek zamanlı modelleme gerektiren sanal

gerçeklik sistemleri, kabin eğitim simülasyonları ve bilgisayar oyunları gibi alanlarda ilerleme sağlanması hedeflenmektedir.

Anahtar Kelimeler: Ekskavatör Simülasyonu, Zemin-Araç Etkileşimi, Doymamış Zeminlerde Zemin-Araç Etkileşimi, Gerçek Zamanlı Simülasyon

To my dear family and friends who helped me to make this real…

ACKNOWLEDGEMENTS

I would first like to thank my thesis advisor Assist. Prof. Dr. Onur Pekcan who always shows exciting ways for me and helps me to walk on that road. His innovative ideas and energetic behaviors became my source of power and enthusiasim to learn new and undiscovered worlds.

I would also like to thank the colleagues, Elife Çakır and Başak Seyisoğlu, who helped me to fix my errors and advice me the right ways during the writing process.

I would like to thank my teammates Ahmet Bahaddin Ersöz and Türker Teke as well. They always tried to help me to write this thesis without pain by providing me enough time and space.

Finally, I must express my very deep gratitude to my parents and to my friends for providing me continuous encouragement and support throughout the process of researching and writing this thesis. This accomplishment would not have been possible without them. Thank you.

TABLE OF CONTENTS

LIST OF TABLES

TABLES

LIST OF FIGURES

FIGURES

LIST OF ABBREVIATIONS

ABBREVIATIONS

CECE	Committee of European Construction Equipment
DEM	Discrete Element Method
ESA	Effective Stress Approach
FEE	Fundamental Earth-moving Equation
FEM	Finite Element Method
GUI	Graphical User Interface
ISVA	Independent State Variables
LWR	Local Weighted Regression
SAE	Society of Automobile Engineers
SWCC	Soil-Water Characteristic Curve
UX	User Experience

LIST OF SYMBOLS

SYMBOLS

f	tool cutting resistance
c	cohesion
c_α	soil to metal adhesion
γ	dry soil's density
γ_{sat}	saturated soil's density
γ_w	unit weight of the water
q	surcharge pressure
b	tool depth
$N_c, N_\gamma, N_q, N_\alpha$	dimensionless Reece factors
L_t	length of the tool under the ground surface
L_f	length of the failure plane
E_M	total measured energy
E_K	kinetic energy
E_P	potential energy
E_D	dissipated energy
E_R	rotational energy
E_T	translational energy
g	gravitational acceleration
ϕ	soil friction angle
K_p	coefficient of passive lateral earth pressure
K_0	coefficient of lateral earth pressure at rest
z	depth of tip from the ground surface
A_s	area of the separation plate
p	cavity pressure
p_0	initial cavity pressure
A_t	tool tip area
B_{fill}	bucket fill ratio
V_{cur}	current volume inside the bucket
V_{cap}	capacity volume of the bucket
W_{bucket}	weight of the bucket
τ	shear strength
σ	normal stress
u	pore water pressure
G	specific gravity of solid particles
S	degree of saturation
e	void ratio
u_a	pore air pressure

χ	a soil parameter depending on the degree of saturation, the soil type, the moisture hysteretic state and the stress conditions
ψ_b	air entry suction
ψ	matric suction
ϕ^b	angle of friction with respect to matric suction
D_r	relative density
χs	suction stress
v	velocity
d	cutting depth

CHAPTER 1

INTRODUCTION

1.1. Problem Statement

Increasing demand in the construction sector creates a requirement for earth removal works. As a natural outcome of this, a large number of excavators are running around the world every day. Among those excavators, hydraulic ones have become more compelling earth-moving machines. A typical hydraulic excavator and parts are shown in Figure 1.1. Like human arm, hydraulic excavator's front manipulator (boom, arm, and bucket) has a capability for flexible movements, which makes it possible to handle earth-moving tasks in a natural and easy way.

Figure 1.1. Hydraulic excavator (Hidromek A.Ş., 2017)

Nowadays, there is a considerable effort to develop more powerful and competent earth-moving systems, i.e., with an increase in the productivity of operators, reduction of the fuel consumption, amplification of the workability of machines and withstanding extreme weather conditions to be used in excavations more effectively. One of the solutions found to achieve this goal is to integrate unmanned (robotic) hydraulic excavators to the construction works. Studies show that with robotic excavators, excavator motions are faster, more power-efficient, and smoother compared to actual excavation performed by a human operator (Kim et al., 2013). To develop an unmanned excavator, accurate prediction of resistive soil forces in real-time is required, which was originally achieved by the experience of operators. In Figure 1.2, a block diagram of a recently introduced autonomous excavation approach is presented in the form of a closed-loop control framework (Dadhich et al., 2016). As clearly understood from this figure, real-time and realistic soil-tool interaction models should be implemented to develop excavator simulations, which can also be used for operator training cabins, computer games, and virtual reality-based systems.

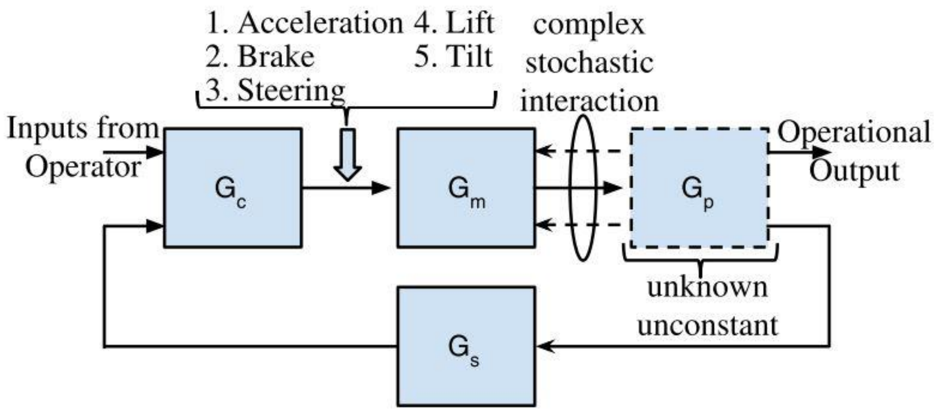

Figure 1.2. Control block diagram of a loading process. Gi is transfer function for i=c (controller), m (machine), p (process/pile) and s (sensors) (Dadhich et al., 2016)

Understanding the behavior of soil-tool interaction for surficial soils with their non-linear behavior is one the most challenging subjects of Geotechnical Engineering field as it requires knowledge from various fields such as Soil Mechanics, Mechanical Engineering and Hydraulic Engineering. This fact was also emphasized by numerous research studies, such as Hemami et al. (1994), Singh (1997), Blouin et al. (2001), William Richardson-Little & C. J. Damaren (2005), etc., conducted to investigate soil-tool interaction behavior.

In fact, a recent study by Xi et al. (2019) highlighted the importance of the weight of the excavation system used in the moon missions. As this can also be extended to Mars missions (Bonitz et al., 2009), every single mass and size increase can result in a tremendous amount of launch and operational costs' increase. The transportation cost approximately covers half of the total mission costs (Boles et al., 1997). Therefore, it is necessary to come up with the a precise and reliable outcome to design the excavation system which will be used on the Moon, Mars or any other out-earth investigations. Another point is that as it is too hard to create an environment like the moon, where gravity is 1/6 of that of Earth's, which has a high vacuum, and extreme atmospheric condition, there is a strong need to eliminate laboratory tests and rely on analytic and numerical methods.

The major challenge is measuring and verifying the performance of excavation tools interacting with the soil, which is generally under the effects of dynamically changing unsaturated soil forces. In essence, three major approaches have been taken to comprehend the soil-tool interaction: (i) laboratory experiments, (ii) analytic methods and (iii) numerical simulations. In addition to very few laboratory works reported in the literature, research studies on this problem successfully yielded various computational methods over the last three decades. Still, the majority of them are too complicated and therefore computationally expensive.

Although with the help of simplifications and generalized formulations, classical methods have a significant role in this area. They are solving problems when one needs real-time excavation models for autonomous excavators (Skonieczny, 2018), but numerical methods such as Discrete Element Method (DEM) and Finite Element Method (FEM) are still computationally expensive and time-consuming. In addition, current analytical methods are not suitable for real-time simulations as they were not developed for solving whole excavation processes, i.e., digging, sweeping, loading, and unloading. Dadhich et al. (2016) stated that even if there were remarkable efforts on developing such models, a decent soil-tool interaction model has not been developed yet.

1.2. Objectives of the Research

With this study,

- accurate prediction of soil-tool interaction force for soils including the effects of water and velocity,
- simulation of soil-tool interaction in real-time (~25 frames/sec),
- covering whole excavation processes (digging, sweeping, loading and unloading),
- realistic visual behaviors for excavated soil,

have been targeted.

1.3. Scope of the Research

A computer program for modeling the soil tool interaction has been established within the scope of the research. This software takes soil types and excavator bucket geometry as inputs, providing flexibility to work on different excavators and soil types. With the help of a joystick (as a controller), excavator's front manipulator (boom, arm, bucket) movements can be controlled in real-time. According to the movement of the bucket, the software calculates and displays forces acting on the excavator bucket. For calculation of resistive soil forces, a novel approach has been proposed, where conventional soil mechanics concepts like Rankine's earth pressure theory and cavity expansion theory are used. Within the scope of this research, additional effects like the existence of water and velocity of the bucket penetrating into the soil are also taken into account.

1.4. Thesis Outline

This thesis consists of five chapters, which start with an introduction of the problem statement, objectives and the scope of this work. The rest of the thesis follows the outline stated below:

- Chapter 2 presents an overview of the literature related to excavation works including the theory of forces and stresses induced around earth moving machines and their modeling.
- Chapter 3 provides the details of the method proposed in this thesis. It provides the fundamentals of equations used to simulate the forces developed around the excavator and the effects of water and velocity. In addition, the stages of the excavation are presented here in detail.
- Chapter 4 presents the simulation tool and its graphical user interface. The results of simulation models and their comparison with the experimental studies are also presented in this chapter.
- Chapter 5 summarizes the main points of this study, highlights the key conclusions and future works related to the modeling work and its applications in the field.

CHAPTER 2

RELATED WORKS

Understanding the fundamentals of excavator soil interaction governs the development of an accurate model depicting field simulations. Within this scope, this chapter mainly provides the related studies to develop the theory for modeling the excavator, the soil and their contact. The chapter starts with outlining the forces acting on the excavator bucket, then provides the essentials of the soil-tool interaction models, illustrating different approaches to fully comprehend the physics of the phenomenon. An extensive set of methods proposed for understanding the mechanism behind soil tool interaction are explained in this section. The proposed methods suffer from various disadvantages: they are challenging to implement in computer environments, their validation is hard to achieve, their precision is quite dependent on the simplifying assumptions, etc.

2.1. Forces Acting on the Excavator

When the excavator is an action, it interacts with the soil through its bucket. Therefore, forces acting on the bucket during the excavation process needs to be well understood. The main sources of these forces are the resistance of soil and the forces applied by the excavator's hydraulics through its boom and arm. The others are generally induced by the interaction through interfaces. Another characteristic of these forces is that they are generally dynamic in nature and generally depend on the physical features of both excavator and bucket, and mechanical properties of soil.

In the literature, forces acting on the bucket are generally divided into categories to investigate them separately. Hemami et al. (1994) defined these five main categories of forces induced on the excavator, all of which need to be considered to advance the excavation process during modeling (Figure 2.1). In this figure, “f_1” is the weight of soil accumulated in the bucket, which changes continuously during an excavation. “f_2” is compacting/passive resistance of soil in front of the bucket surface. If there is no action for pushing and/or compacting the soil in front of the bucket blade, then it becomes zero. “f_3” is the force generated by friction between soil and bucket walls. The direction of the force is the same as the velocity vector. “f_4”is the force required to shear the soil, which is mainly responsible for cutting the soil to be excavated. Finally, “f_5” is the force required to move (raise) the portion of the soil material in front of the bucket, which is displaced by the buckets’ movement. Although all forces are generally required for precise modelling of soil tool interaction, Hemami et al. (1994) stated that f_3 and f_5 could be ignored in calculations when their magnitude and corresponding effects are compared to other ones.

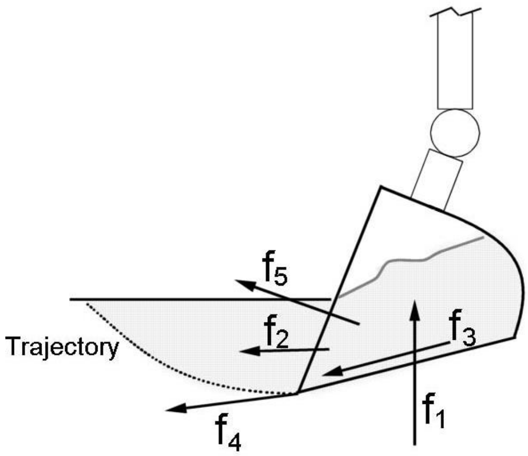

Figure 2.1. Five main forces acting on a bucket during excavation (Hemami et al., 1994)

The next sections summarize some of the previous studies commonly referred in the literature. It is important to note that although they were performed to solve soil-tool interaction problem covering the critical forces, most of them are very complex models which are generally computationally expensive and/or impractical for real-time automatic control. Moreover most of them do not cover the whole excavation processes (digging, sweeping, loading, and unloading).

2.2. Fundamental Earth-moving Equation (FEE)

Fundamental Earth-moving Equation (FEE) is aimed to observe the resistive forces exerted by soil to wide cutting blade taking into consideration of soil and blade properties. Soil's cohesion, weight, frictional elements and adhesion between soil and blade are analyzed in order to compose a formula that can calculate resistive forces more accurately. The Fundamental Earth-Moving Equation presented by Reece's (1964) is given in Eq. 2.1,

$$f = cbN_c + \gamma b^2 N_\gamma + qbN_q + c_\alpha b N_\alpha \tag{2.1}$$

where;

f: tool cutting resistance (N/m),
c: cohesion (N/m^2),
c_α: soil to metal adhesion (N/m^2),
γ: soil's density (N/m^3),
q: surcharge pressure (N/m^2),
b: tool depth (m),
N_c, N_γ, N_q, N_α: factors of cutting angle, soil failure angle, tool-soil friction angle and soil friction angle, respectively.

This equation was formed based on Terzaghi's Bearing Capacity formula. It is a suitable way to solve the resistive force on a wide cutting blade, and generally beneficial for bulldozers. However, there are some accuracy problems when it comes to excavators and movement of the bucket.

2.2.1. Extended Fundamental Earth-Moving Equation

FEE is valid for flat blades moving horizontally in the soil and cannot be applied to sloped terrains. The reason behind this is that FEE was developed for agricultural tools which generally work on horizontal surfaces. However, in the case of excavation, the terrain is usually sloped and the soil is captured by blade accumulation. Cannon (1999) made some modifications on the FEE in order to make the equation applicable to sloped soil environments.

In FEE, as the flat blade moves, material that slides along the failure surface creates a wedge as shown in Figure 2.2. To find the forces that affect the soil-tool behavior, the failure surface is approximated as a plane. The resulting forces acting on the wedge are defined as in Figure 2.3,

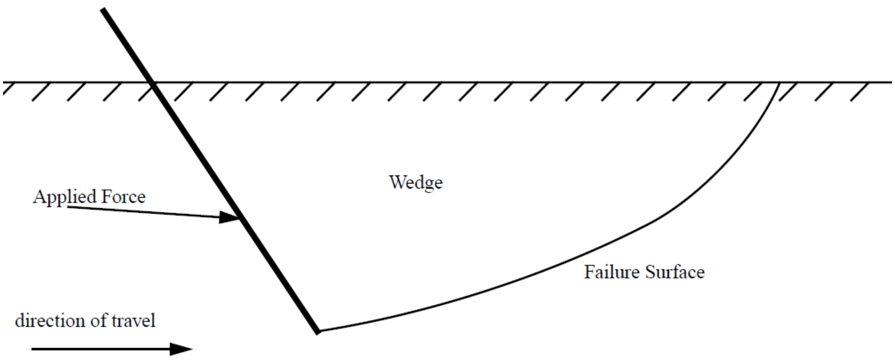

Figure 2.2. The wedge created by the forces generated by the movement of the flat blade (Cannon, 1999)

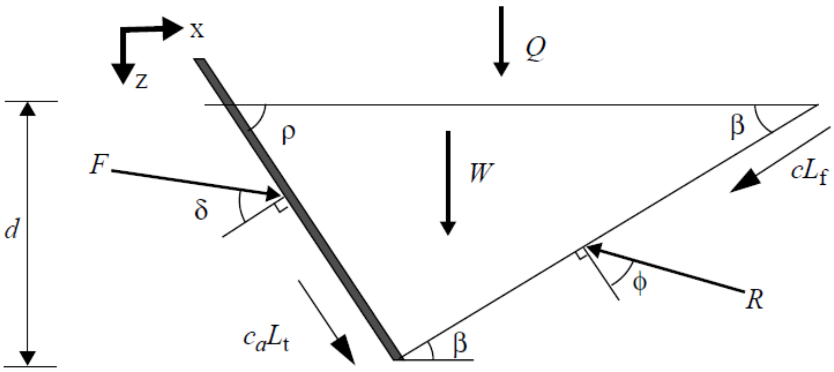

Figure 2.3. Forces acting on the wedge (as cited in Cannon, 1999)

where:

R: reaction force of the soil against the sliding wedge,

W: weight,

Q: the surcharge force,

c_aL_t: the adhesion force of the soil acting on the tool,

cL_f: the shear force of the material away from itself, which is a function of the cohesiveness of the material,

F: force exerted by the tool against the wedge.

The equation describing F in the original FEE (Eq. 2.1) is rearranged as;

$$F = \left(\gamma g d^2 N_\gamma + c d N_c + q d N_q\right) w$$

$$N_\gamma = \frac{cot\rho + cot\beta}{2[\cos(\rho+\delta) + \sin(\rho+\delta)\cot(\beta+\phi)]}$$

$$N_c = \frac{1 + cot\beta\cot(\beta+\phi)}{\cos(\rho+\delta) + \sin(\rho+\delta)\cot(\beta+\phi)}$$

$$N_q = \frac{cot\rho + cot\beta}{\cos(\rho+\delta) + \sin(\rho+\delta)\cot(\beta+\phi)} \qquad (2.2)$$

The changes made in the original FEE are outlined as follows;

- Instead of being distributed evenly over the wedge, the surcharge is assumed to be only on the bucket side of the bucket tip (Figure 2.4). The surcharge (Q) and the weight of the soil behind the bucket tip (W_1) form swept volume (V_s) which is shown in the shaded area in Figure 2.4.

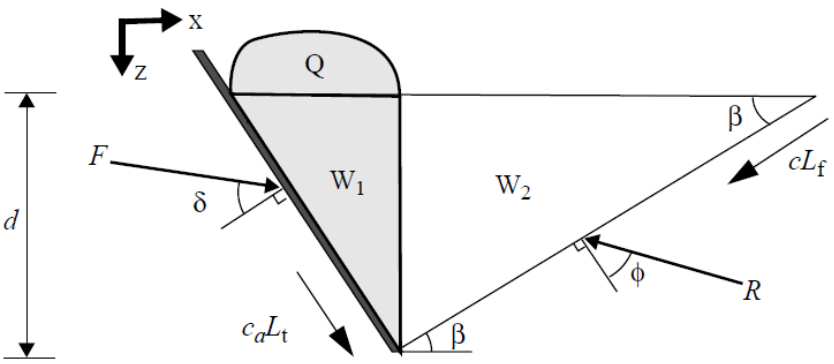

Figure 2.4. Wedge model that accounts for the material being retained in the bucket (Cannon, 1999)

- The slope of the terrain is taken into consideration. Force distribution of the sloped terrain can be seen in Figure 2.5.

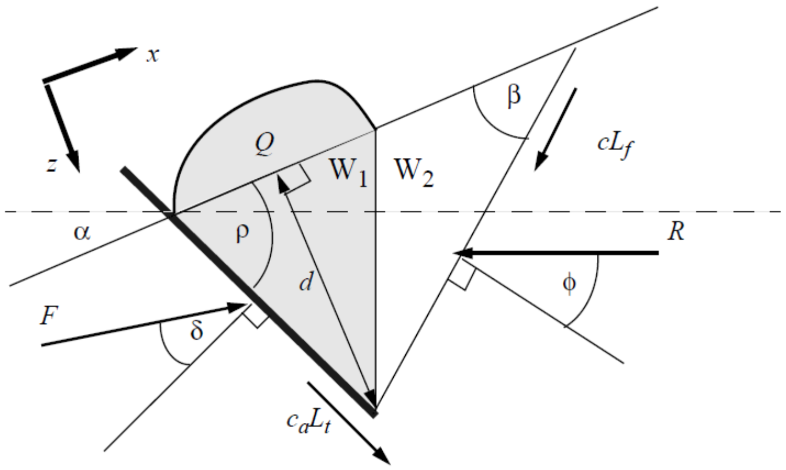

Figure 2.5. Wedge model that accounts for the material being retained in the bucket, on sloping terrain (Cannon, 1999)

Then the modified version of the FEE becomes;

$$F = \left(d^2 w\gamma g N_w + cwdN_c + V_s\gamma g N_q\right)$$
$$N_w = \frac{(cot\beta - tan\alpha)(cos\alpha + sin\alpha\cot(\beta+\phi))}{2[\cos(\rho+\delta)+\sin(\rho+\delta)\cot(\beta+\phi)]}$$
$$N_c = \frac{1 + cot\beta\cot(\beta+\phi)}{\cos(\rho+\delta)+\sin(\rho+\delta)\cot(\beta+\phi)}$$
$$N_q = \frac{cos\alpha + sin\alpha\cot(\beta+\phi)}{\cos(\rho+\delta)+\sin(\rho+\delta)\cot(\beta+\phi)} \quad (2.3)$$

2.2.2. FEE-Based Models

After the proposal of FEE and its modifications, a large number of FEE-based models were developed to obtain soil-tool interaction forces accurately. These models provide equations to obtain the draft force with different combinations of the critical forces explained at the beginning of this chapter. They differ from each other depending on the forces considered in the model (Skonieczny, 2018).

Table 2.1. *FEE-based models and the key forces they include* (Skonieczny, 2018)

FEE-based model	*Gravity*	*Cohesion*	*Surcharge*	*Adhesion*	*Inertia*
Reece, 1964	√	√	√	√	
Shazali, Osman, 1969	√	√	√	√	
Gill & Vandenberg, 1968	√	√			√
Godwin & O'Dogherty, 2007	√	√	√	√	
Zelenin, Balovnev, & Kerov, 1992	√	√	√		
McKyes, 1985	√	√	√		
Swick & Perumpral, 1988	√	√	√	√	√
Willman & Boles, 1995	√	√			

These forces described in Table 2.1 are explained below:

- **Gravitational Force**: Gravitational force is one of the significant forces when moving the earth surface is considered. Almost all force equations include gravitational force and forces related to it. For the Swick and Perumpral method which includes all the key forces, it is obvious that gravity (in terms of depth) is the most significant component when calculating total force (Wilkinson & DeGennaro, 2007).

- **Cohesion**: Movement of the earth surface is simply due to shearing of the soil and shear force is directly related to the cohesion. This parameter is used in all draft force models and actively contributes to the total force. The total resistive force increases with the increase in cohesive force. Figure 2.6 shows the variation of the total force in soil with zero and non-zero cohesion (Tsuji et al., 2012).

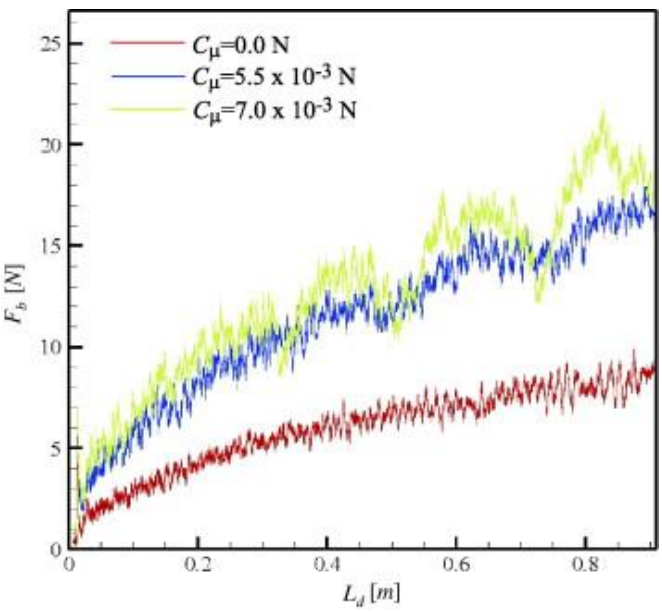

Figure 2.6. Total resistive force vs. lateral excavation distance in different cohesive force parameters (Tsuji et al., 2012)

- **Adhesion**: Soil adhesion between soil and tool generated by Laplace pressure and meniscus tension (Tong et al., 1994). In the calculation of the total draft force, as the buckets have an almost smooth surface, its contribution is smaller when comparing the cohesion and surcharge loads. Therefore, some of the methods do not include this effect (Hettiaratchi et al., 1966).

- **Inertial Force**: Inertial force becomes significant for the soil-tool interaction when cutting speed is high. However, excavations are done at low speeds in general, therefore, it can be omitted (Wheeler & Godwin, 1996). Table 2.1 also shows that most of the models do not include the inertial force.

- **Surcharge Force**: As the tool proceeds and accumulates the soil, soil presses down the cutting plane and the total draft force increases. For the cohesionless soils, surcharge force exponentially increases throughout the cutting phase and becomes the most significant contributor to the total resistance force. Therefore, it is not reasonable to neglect this key force (Skonieczny, 2018).

2.3. Energy Dissipation Method

The energy dissipation method (Vahed et al., 2008) mainly focuses on the soil deformation, considering different soil types and geometry of the soil disturbed by the excavators. To understand the behavior of the soil during the excavation process, an energy-based algorithm was used. The advantage of this method is that there is no need to deal with the complicated modeling of forces. The model relies on the measured energy formula, which is created directly by measurements. The total measured energy formula (Eq. 2.4) is shown below;

$$E_M = E_K + E_P + E_D \tag{2.4}$$

where E_M indicates the total measured energy, E_K is the kinetic energy, E_P stands for potential energy, and E_D indicates dissipated energy.

The total measurement energy can be calculated using the measurements of bucket force in the sweeping phase, in which bucket moves along a straight line. E_M can be integrated by the simple work formula (Eq. 2.5), where the work is calculated by integrating the force F(x) over displacement x;

$$W_{ab} = E_M = \int_b^a F * dx \tag{2.5}$$

The area under the graph in Figure 2.7 is used to find energy.

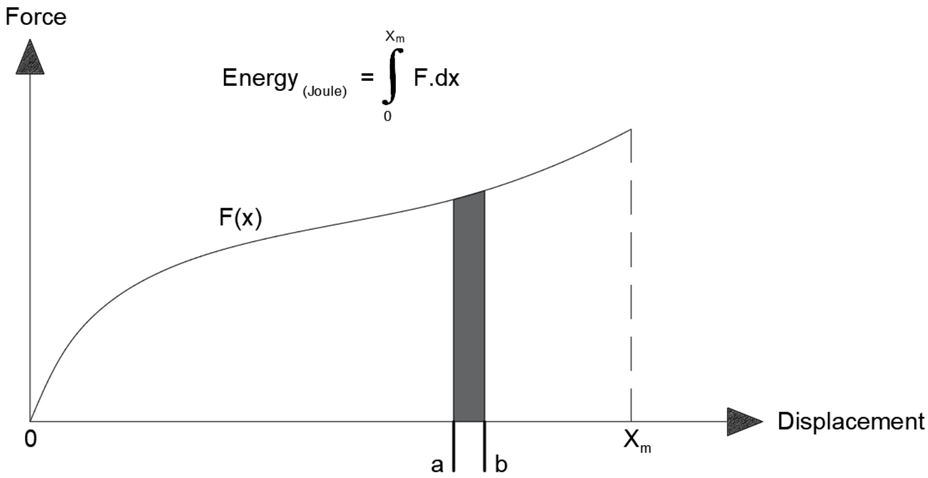

Figure 2.7. Energy as the integral of force versus displacement (Vahed et al., 2008)

To obtain input energy for storing the data in an array of E_M, energy can be approximated by using the Trapezoidal Rule (Eq. 2.6);

$$W_{ab} = E_M = \frac{(x_n - x_{n-1}) * (F_n - F_{n-1})}{2} \tag{2.6}$$

where n is the sampling interval.

The general kinetic energy formula (Eq. 2.7) is;

$$E_K = E_R + E_T \tag{2.7}$$

where E_R is the rotational energy, and E_T denotes translational energy.

Because sweeping phase is assumed to be a horizontal straight line, rotational energy is neglected when calculating the kinetic energy.

$$E_K = E_T = \frac{1}{2} m V^2 \tag{2.8}$$

To approximate the kinetic energy, mass and velocity arrays should be created. They can be formed by the formulas (Eq. 2.9, and Eq. 2.10) below;

$$V_{ab} = V_n = \frac{(x_n - x_{n-1})}{T_s} \tag{2.9}$$

where T_s is the sampling period.

$$Mass_{(n)} = E_M = \frac{(x_n - x_{n-1}) * (H_n + H_{n-1})}{2} * l * \gamma \tag{2.10}$$

where H is vertical displacements, l indicates constant bucket width, and γ stands for the soil density.

Based on the equations above, the kinetic energy (Eq. 2.11) at any sampling interval can be calculated by;

$$E_K = \frac{1}{2}\left(\frac{(x_n - x_{n-1}) * (H_n + H_{n-1})}{2} * l * \gamma\right)V^2 \qquad (2.11)$$

To find the potential energy limit equilibrium algorithm is used. During on-line estimation, the potential energy of any sample can be found using the equation below (Eq. 2.12);

$$E_P = mgh \qquad (2.12)$$

The accumulated mass is calculated above using Eq. 2.10 and the estimated height "h" can be found using limit equilibrium analysis.

$$E_P = \left(\frac{(x_n - x_{n-1}) * (H_n + H_{n-1})}{2} * l * \gamma\right)gh \qquad (2.13)$$

The dissipation energy can be found by reversing Eq. 2.4;

$$E_D = E_M - E_P - E_K \qquad (2.14)$$

where E_M is measured, and E_P and E_K can be calculated using Eq. 2.11 and Eq. 2.13.

From the dissipation energy formula, resistive force can be calculated using work-energy theorem. With all the equations outlining the components of energy, this method is a practical one to investigate the behavior of the soil during excavation. Using the above relations, the observation process of the soil–bucket relationship is simplified. However, the disadvantage of this method is that it only observes the soil movement during the sweeping phase. The entire trajectory of the bucket in the soil is not taken into consideration. Although this method is advantageous during the sweeping phase of the excavation, it is not useful when it comes to other phases of the bucket movement.

2.4. Learning-Based Method

The aim of learning-based method (Singh, 1995) is to invent methods for a robot to find resistive forces during excavation, starting from the analysis of a flat blade's movement in soil and to improve this analysis iteratively to find the movement of an excavator. In this method, a sensor-equipped excavation robot can determine the soil properties and excavate a specific amount of soil. In addition, inclination and the uneven composition of the terrain are also taken into consideration. To analyze the resistive forces of an excavator bucket in uneven terrain, an experimental system consisting of a hydraulic robot with an excavator bucket, a force sensor, a sandbox and a laser range scanner to produce an elevation map of the terrain, were set up (Figure 2.8). Data collected from this experiment were used to form a function approximation scheme that can predict resistive forces.

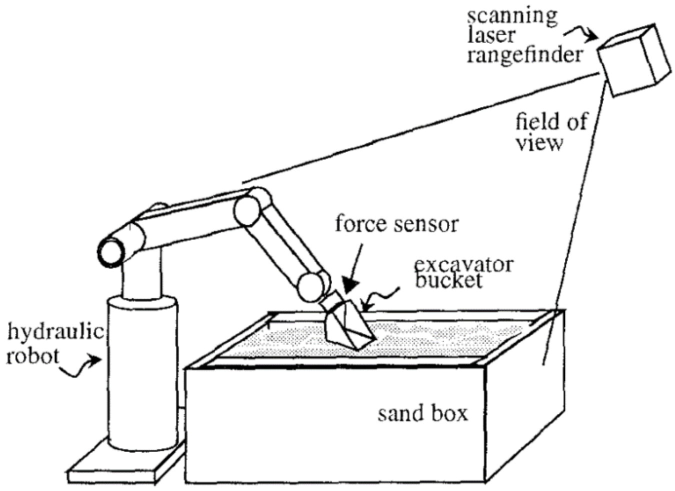

Figure 2.8. Testbed (Singh, 1995)

In learning based method, an equation to predict the resistive forces was proposed;

$$A_1k_1 + \cdots + A_nk_n + W_1k_{n+1} + \cdots + W_mk_{n+m} = F \qquad (2.15)$$

where F stands for resistive forces, A implies robot's action, W is the world's state, and the pair of *n* and *m* is the number of variables needed to encode *A* and *W*, respectively.

The shape of the terrain shown in elevation map that is formed by the laser range scanner is recorded while the excavator bucket moves along a path. The system parameters can be interpreted more easily from Figure 2.9.

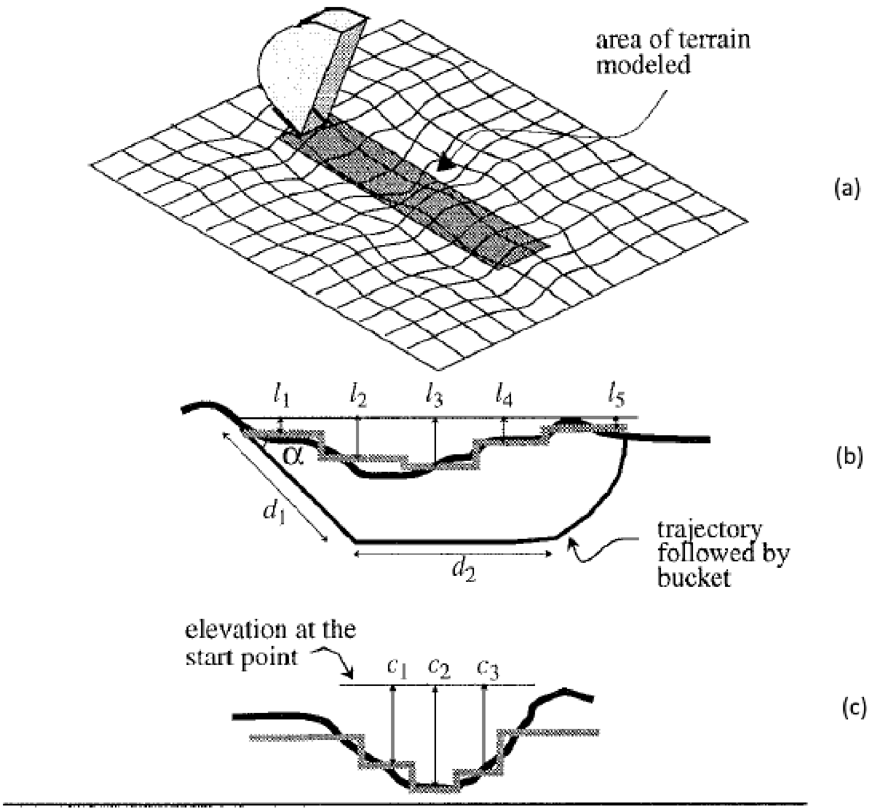

Figure 2.9. State of terrain and elevation profile. (a) only part of the terrain is represented. An excavation trajectory is represented by a, d_l, d_2 in (b). The world state is represented by a linearized elevation profile, l_i, along the trajectory (b) to be excavated and across the excavated area, c_i, in (c) (Singh, 1995)

For every dig, α and l_i are fixed, and the values of d_1, d_2, c_1, c_2, c_3 can be different from the previous dig. For each dig, the force readings, α, l_i, d_1, d_2, c_1, c_2, c_3 are stored in an array named as G. G was improved with the knowledge gained from the examination of the mechanics of excavation.

Some learning methods are used to approximate the resistive force F. In memory-based learning; there are local models from which data can be approximated. Local Weighted Regression (LWR) was used in this method to get an approximated data graph. It is known that the approximations of local models are more accurate than global models' ones.

Another learning method used in this approach is the back-propagation neural network method. In this method, sample inputs and true outputs were shown to a network to achieve the network to learn by adjusting its weights. Although this is an accurate way to predict forces acting on excavator bucket surface, it is not a practical way or applicable on simulation environment.

CHAPTER 3

EXCAVATOR – SOIL MODEL

Considering the disadvantages and complexities of the models proposed in the literature, this study proposes a new method for the modelling of soil-tool interaction. This chapter presents the details of the implemented method to accurately model excavator soil interaction (also referred to as soil - tool model) and to apply it to the practical problems encountered in the field. The chapter starts with the fundamental assumptions and presents the equations necessary for modelling of soil considering the near surface effects including velocity and water. It also includes the phases of excavation together with the geometric details of the excavator bucket.

3.1. Force Prediction

Major forces acting on the excavator bucket during the excavation process are summarized in Chapter 2 of this thesis. The forces f_1, f_2, and f_4 presented in Figure 2.1 are active forces due to bucket weight, compacting resistance, and cutting force, respectively. The method proposed in this study solves compacting resistance with lateral earth pressure theory and cutting force with cavity expansion theory. Moreover, the excavation process is divided into several phases where different forces become effective on different phases.

3.1.1. Excavation Phases

Excavation phases can be defined as states of the excavator bucket in soil creating different kinds of forces during the excavation process. To develop more accurate excavator simulations, excavation processes must be examined more realistically.

Although there are some studies in the literature to outline these phases (Blouin et al., 2001; Kim et al., 2013; Park, 2002), they do not adequately address the excavation process. As a result of the observations made at the construction sites (Figure 3.1), it is seen that the excavation process consists of four main phases, which are (i) digging, (ii) sweeping, (iii) loading, and (iv) unloading, in the order of occurrence. Considering the prediction of forces, in this chapter, only the first three phases, presented in Figure 3.2 are discussed. Since unloading phase is more related to the visualization than rather the force prediction, this phase is covered in the visualization part.

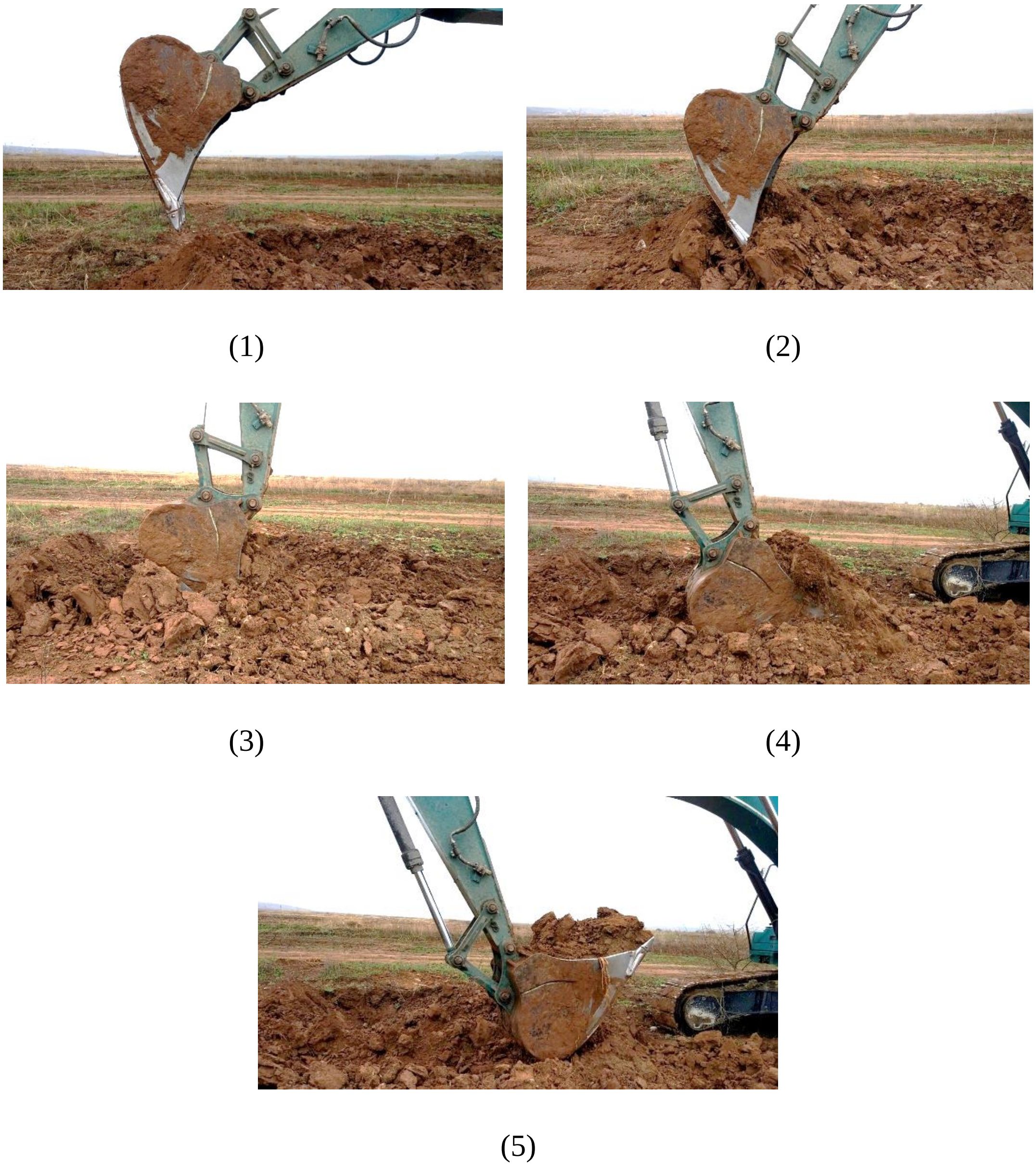

Figure 3.1. Observation on excavation phase in the field
(1) initial state, (2) digging, (3) sweeping, (4) loading, (5) final state

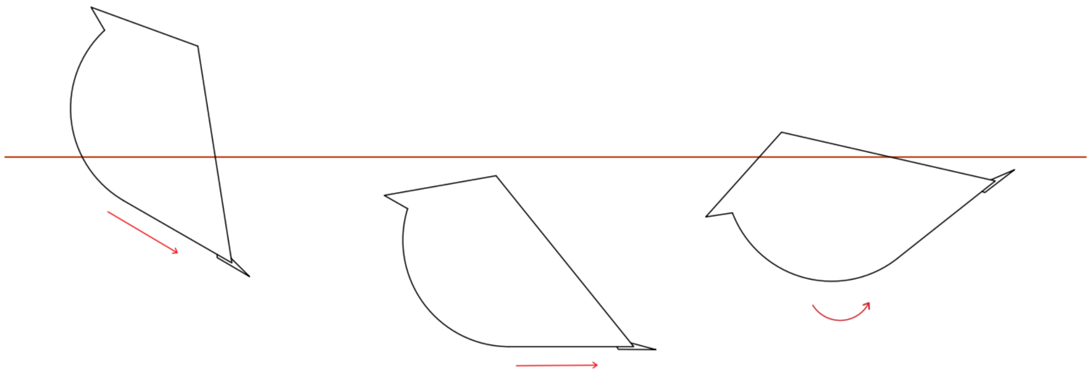

Digging (2) | Sweeping (1) (2) (3) | Loading (1)* (2)* (3)

<u>Active Forces</u>

1. Passive Lateral Earth Pressure
2. Cavity Expansion Pressure
3. Weight

* Linearly decreasing

Figure 3.2. Excavation phases and active force components on each phase

There are three main forces acting on the excavator bucket, which are listed as (1) passive lateral earth pressure, (2) tip resistance, and (3) soil weight. In this thesis, cavity expansion theory is used to calculate the tip resistance, as will be explained in Section 3.1.4. Since the shear stress and the frictional forces are included in the formulation of cavity expansion theory, they are not considered separately when modeling excavation phases. There are mainly two considerations behind the designation of main forces that act during the excavator bucket-soil interaction, namely the movement of the bucket and the properties of the soil. These are further explained for each phase in the following parts.

Phase 1: Digging

Digging phase can be described as penetration of the bucket to the soil until the bucket reaches the desired depth. In this phase, the bucket does not move the soil in the horizontal direction. Therefore, passive lateral earth pressure does not act as a bucket force. Separation of the soil occurs in this phase, however, the soil is not accumulated in the bucket. Hence, the soil weight is not considered in the calculation. As the soil failure plane has not been formed yet on the trajectory of excavation tool, excavator bucket separates the soil, and this separation causes a tip resistance, which makes the tip resistance to be the only force affecting the soil-bucket interaction model. In short, there is only one active force in digging phase, tip resistance denoted with number (2).

Phase 2: Sweeping

In the sweeping phase, excavation tool moves laterally to separate the soil and accumulate the material in the bucket. As in digging phase, bucket tip travels through virgin soil zone. For that reason, tip resistance has an impact on soil-tool interaction. The horizontal movement of the excavation tool causes the formation of the passive-lateral earth pressure because the soil in front of the excavator bucket resists against bucket motion. Soil accumulates in excavator bucket and to carry the accumulated soil, excavation tool creates a force against soil weight, which means that the soil weight also affects the soil-tool interaction. To summarize, the forces denoted as (1), (2), and (3) are all acting in sweeping phase.

Phase 3: Loading

In this phase, the bucket makes a rotation movement to accumulate and carry the excavated soil. Therefore, soil weight is the primary force effect on the bucket. It is assumed that as the bucket rotates, where bucket tip starts to point upwards, bucket tip resistance and lateral earth pressure decrease linearly and become zero when the bucket tip reaches to ground surface. For the bucket tip resistance, the movement where bucket tip travels horizontally in virgin soil zone changes and with rotation, soil tip starts to travel in the already-failed zone. For simplicity, it is assumed to be a linear change in bucket tip resistance. For the lateral earth pressure, lateral movement of soil continue at the bottom level with rotation and stops at the top level. Besides, the bucket's bottom plate separates excavated soil from the subgrade when the rotation is completed. Therefore, lateral earth pressure also becomes zero when the separation is completed. Again, it is assumed that the decrease in lateral earth pressure in the loading phase is linear. In short, similar to sweeping phase, the active forces in the loading phase are (1), (2), and (3) in the loading phase. The only difference is that forces (1) and (2) are linearly decreasing in this phase.

3.1.2. Soil Parameters

Soil parameters, undoubtedly, have a significant effect on soil behavior and its response during the excavation process. The simulation, should accept different combinations of soil parameters and provide reliable results. To more realistically model widely encountered soils in the field, in this study, sand and clay types of soils are mainly considered. For practical purposes, there are some ranges defined for soil parameters for specific soil types. For clayey soils, there are five soil types taken into account, which are very soft, soft, medium stiff, stiff, and very stiff. Similarly, for sandy soils, there are five soil types ranging from are very loose, loose, medium dense, dense, and very dense. The initital engineering properties, which are imaginary, of each soil type are provided in Table 3.1.

Table 3.1. *Soil parameters used for simulation*

Soil Type	γ (kN/m^3)	γ_{sat} (kN/m^3)	c' (kPa)	ϕ' (°)
Clayey Soils				
Very Soft	16	18	0.1	16
Soft	17	19	5	18
Medium Stiff	18	20	8	20
Stiff	19	21	10	22
Very Stiff	20	22	15	24
Sandy Soils				
Very Loose	15	16	0.1	28
Loose	16	18	0.1	29
Medium Dense	18	19	0.1	33
Dense	20	22	0.1	39
Very Dense	21	23	0.1	41

3.1.3. Lateral Earth Pressure

Lateral earth pressure is the pressure that soil applies in the horizontal direction, which depends on the movement experienced by the tool in the soil. The term passive lateral earth pressure demonstrates the lateral earth pressure when the tool moves into the soil, which compresses the soil mass. When the bucket of the backhoe excavator is moved through the material, the soil in front of the bucket will try to resist the movement. While cutting the soil, these resistive forces can be calculated through the passive lateral earth pressure as their behavior is very similar.

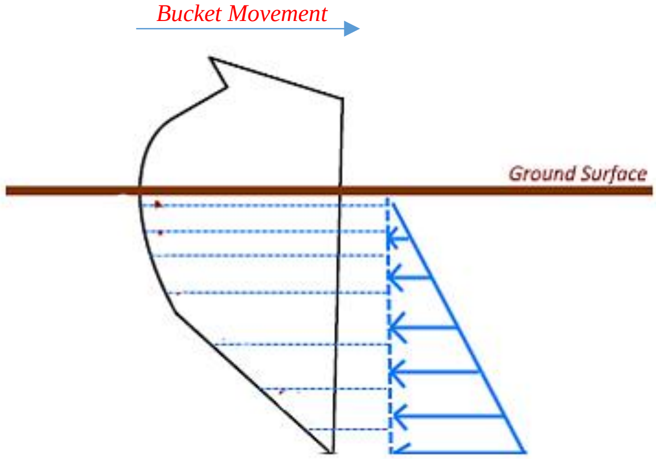

Figure 3.3. Representation of passive lateral earth pressure

In the literature, two methods are accepted to determine passive lateral earth pressure, which are:

(i) Coulomb's Passive Lateral Earth Pressure Theory, and

(ii) Rankine's Passive Lateral Earth Pressure Theory.

Coulomb's Passive Lateral Earth Pressure Theory is also known as the limit equilibrium approach, which was proposed for retaining structures by Coulomb (1776). This approach calculates lateral earth pressures through the equilibrium of forces acting on the earth retaining systems. Generally, frictional force between the soil and structure, cohesion of the material itself, adhesion happening between material and structure, weight of the structure, and resistive force of the soil against structure form the basis of these equilibrium calculations. Coulomb found the coefficient of passive lateral earth pressure as in Eq. 3.1.

$$K_p = \frac{sin^2(\alpha - \phi)}{sin^2\alpha \, sin(\alpha + \delta)\left[1 - \sqrt{\frac{sin(\phi + \delta) sin(\phi + \beta)}{sin(\alpha + \delta) sin(\alpha + \beta)}}\right]^2} \qquad (3.1)$$

where ϕ is the angle of friction between material-material, δ is the interface friction angle between material-structure, α is the angle of the interface from the horizontal, between structure and material, and β is the angle of backslope.

Rankine's Passive Lateral Earth Pressure Theory, unlike Coulomb's Theory, assumes the structure is frictionless, i.e., $\delta = 0°$, and the interface between material and structure is vertical, i.e. $\alpha, = 90°$. In addition to these assumptions, when the angle of backslope is zero, i.e., $\beta = 0°$, the equation to calculate the coefficient of passive lateral earth pressure can be simplified in Eq. 3.2.

$$K_p = \frac{1 + sin\phi}{1 - sin\phi} \tag{3.2}$$

Coulomb's Theory does not calculate the passive resistance correctly, which comes with an error on the unsafe side as it fails to predict the geometry of the curved failure surface (Knappett & Craig, 2012). Therefore, Rankine's Theory is used to predict lateral resistance during horizontal movement of the excavator bucket.

Formulation of the Rankine Passive Lateral Earth Pressure (Rankine, 1891) is given as:

$$\sigma_p{}' = \sigma_z{}'K_p + 2c'\sqrt{K_p} \tag{3.3}$$

where $\sigma_p{}'$ is passive lateral earth pressure, $\sigma_z{}'$ is effective vertical stress, K_p is the coefficient of passive lateral earth pressure, and c' is cohesion parameter of soil.

The purpose behind the usage of the effective vertical stress and drained domain in the case of soil cutting is explained by McKyes (1985) in *"Soil Cutting and Tillage"* through two main reasons. The first reason is that excavation operations are mostly done in the upper layer of the soil. Because upper layer is not generally saturated, total strength parameters are not convenient for the excavation process. The second reason is that in the case of undrained saturated fine-grained soil the effective friction angle (ϕ') is predicted with an error, which means assuming a wrong failure plane in the soil body (Figure 3.4). Consequently, soil cutting forces and volumes can be calculated incorrectly**.**

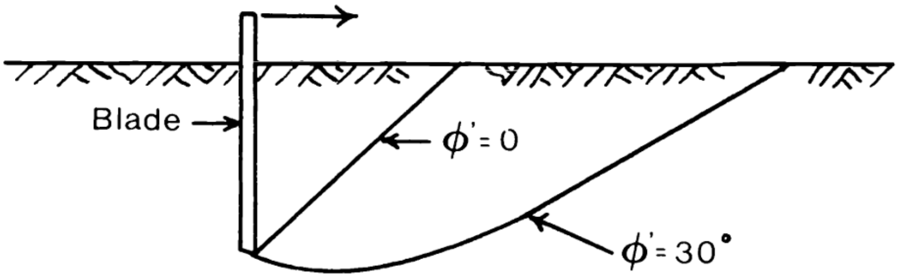

Figure 3.4. Different failure planes for different angle of friction values (McKyes, 1985)

3.1.4. Tip Resistance

Tip resistance of an excavator bucket is an important component when examining bucket forces. According to Park (2002), penetration force (R_p) is formed by the addition of bucket teeth resistance (R_{pt}) and separation plate resistance (R_{ps}). The formulation of the penetration force is given in Eq. 3.4.

$$R_p = R_{pt} + R_{ps} \tag{3.4}$$

Separation plate resistance has a formula (Eq. 3.53.5) that combines the normal pressure (p_n) acting on the plate with adhesional (c_a) and frictional (δ) force elements.

$$\mathrm{R}_{ps} = \mathrm{R} = q_s\, A_s = (c_a + p_n \tan\delta\,) A_s \qquad (3.5)$$

where $p_n = \gamma z$ when separation plate is horizontal, $p_n = K_0 \gamma z$ when separation plate is vertical, A_s is area of the separation plate, z is the depth of tip from the ground surface, K_0 is lateral earth pressure coefficient at rest.

The bucket teeth resistance (R_{pt}) is the part that is related to the tip resistance. There are some discussions about whether the bearing capacity method or the cavity expansion method should be used when studying tip resistance where both methods have their own advantages and disadvantages (Mayne et al., 1999). Cavity expansion method is chosen for investigating the tip resistance in this study. The excavator bucket-soil penetration usually happens at an inclined surface where in bearing capacity theory, the tool is assumed to be penetrating the soil in a perpendicular direction. Therefore, bearing capacity theory is not used for the tip resistance calculation.

Cavity expansion theory overcomes all the disadvantages of the bearing capacity theory. It is used for observing how a cavity grows and how much force is needed to enlarge it while penetrating the soil. Also, the inclination of the surface is not a problem when using cavity expansion theory thanks to the abilities of the theory to be applied any arbitrary angle.

Cavity expansion theory assumes the device that forms the cavity to be spherical or cylindrical. Therefore, in the calculation process of the resistance of a bucket tip, some approximations concerning the shape of cavity have to be made as shown in Figure 3.5.

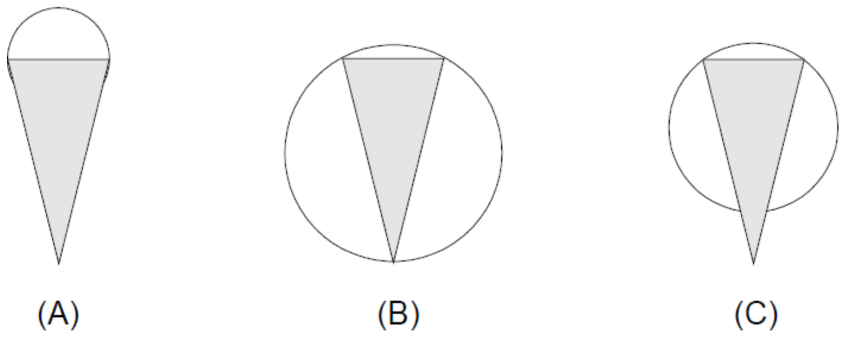

Figure 3.5. Approximations concerning cavity shape (Park, 2002)

In approximation A, the cavity is not large enough to take into consideration of the bucket teeth but only large enough to measure the area on the top of the bucket teeth. In approximation B, the cavity approximation is too large compared to the real bucket teeth cavity. The approximation C is a better option because it is not too large or too small. It is an approximation in between A and B, and it is the one used in this study.

In the cavity expansion process, the initial values of the radius a_0 and pressure p_0 are not provided, therefore an assumption is needed (Figure 3.6). These initial assumptions are;

$$a_0 = 0$$
$$\mathrm{p}_0 = \frac{\sigma_1 + \sigma_2 + \sigma_3}{3} \qquad (3.6)$$

where $\sigma_1, \sigma_2, \sigma_3$ are the stress acting on the bucket tip in all three directions.

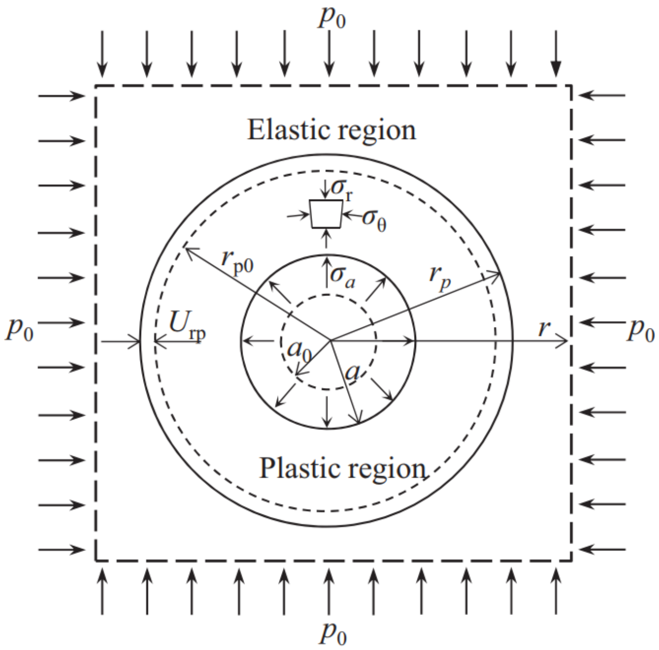

Figure 3.6. Cavity expansion model (Li et al., 2016)

To solve this problem, the process of the penetration of the bucket teeth to soil should be examined thoroughly as can be seen in Figure 3.7.

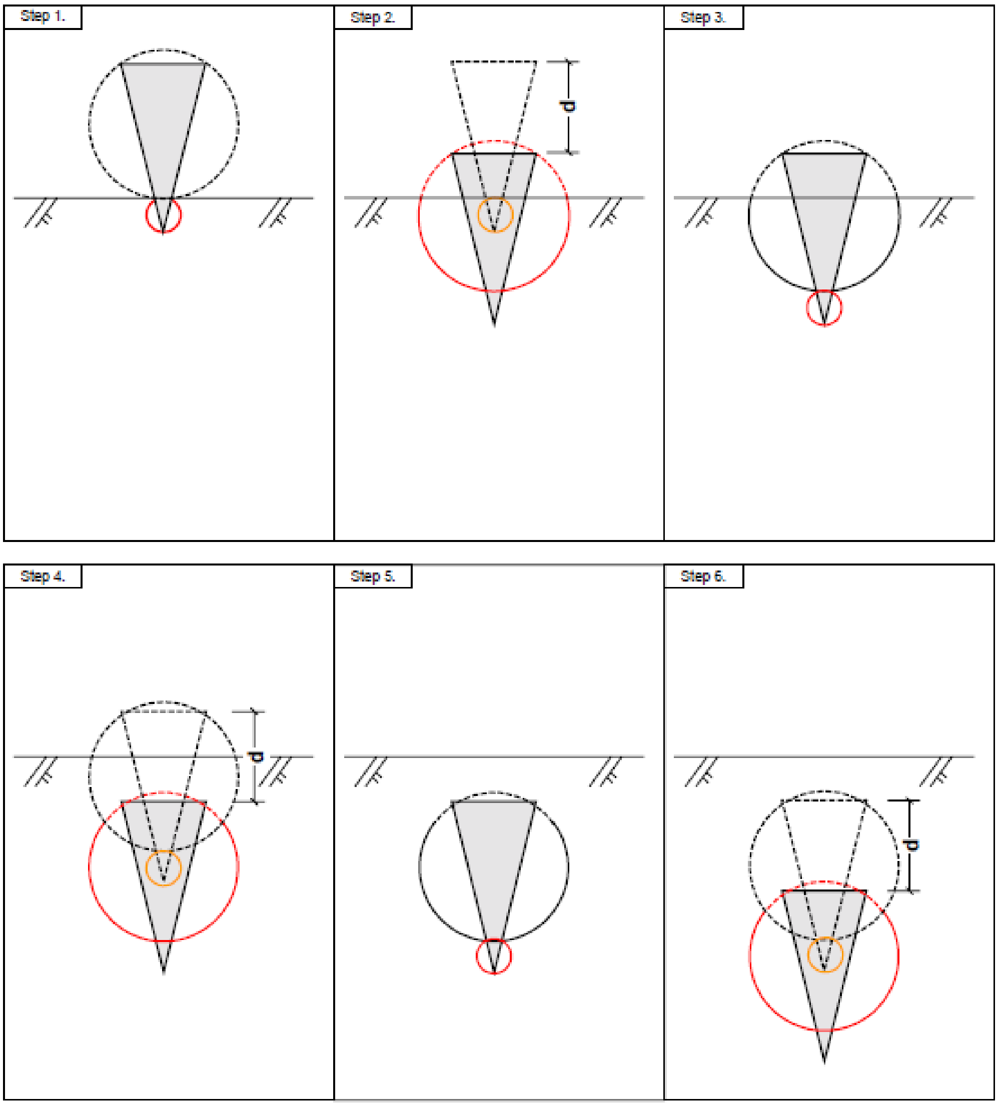

Figure 3.7. Steps of the bucket teeth penetration process (Park, 2002)

In step 1, only the bucket teeth are penetrating to the soil. Initial cavity a_0 is marked by a red circle and the initial pressure p_0 is the earth pressure at rest. As the bucket teeth proceed to penetrate in step 2, initial cavity starts to grow and expand until it reaches to the red circle's size. The cone penetrates to soil at depth d. In step 3, the cone tip marked by the smaller circle is now taken as another initial cavity a_0 for the step 4. In step 4, it can be seen that the initial cavity grows for bucket teeth to be fully in the soil and takes the shape of the approximation C. In steps 5 and 6, earlier steps are simply repeated.

The formula used for the bucket teeth resistance (R_{pt}), presented in f, using cavity expansion theory can be written as (Eq. 3.7);

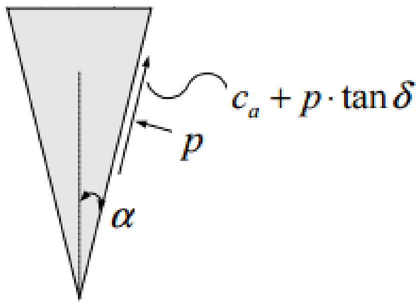

Figure 3.8. Bucket teeth resistance (Park, 2002)

$$\mathrm{R}_{pt} = \mathrm{n}\, q_t\, A_t = \mathrm{n}[\mathrm{p} + (c_a + \mathrm{ptan}\delta\,) cot\alpha] A_t \qquad (3.7)$$

where n is the number of teeth, p is the cavity pressure, c_a is adhesion, δ is the friction angle, α is tip semi angle, A_t is tip area. The formula of the cavity pressure p (Eq. 3.8) is;

$$p = \frac{(\mathrm{m}(\mathrm{Y} + (\mathrm{a} - 1)\, p_0))}{(m + a)} \qquad (3.8)$$

where m is equal to 1 for a cylindrical cavity, 2 for a spherical cavity.

$$Y = \frac{2 * c * cos\phi}{1 - sin\phi} \qquad (3.9)$$

$$a = \frac{1 + sin\phi}{1 - sin\phi} \tag{3.10}$$

$$p_0 = \sigma'_v = \gamma' * z \tag{3.11}$$

3.1.5. Bucket Fill Ratio and Bucket Weight

During the digging process, current bucket fill ratio is continuously calculated by dividing current soil volume inside the bucket to the maximum capacity volume (Eq. 3.12). Current soil volume inside the bucket is equal to multiplication of the bucket width and the area between trajectory line (generated by bucket tip path) and the ground level, which is shown in the Figure 3.9.

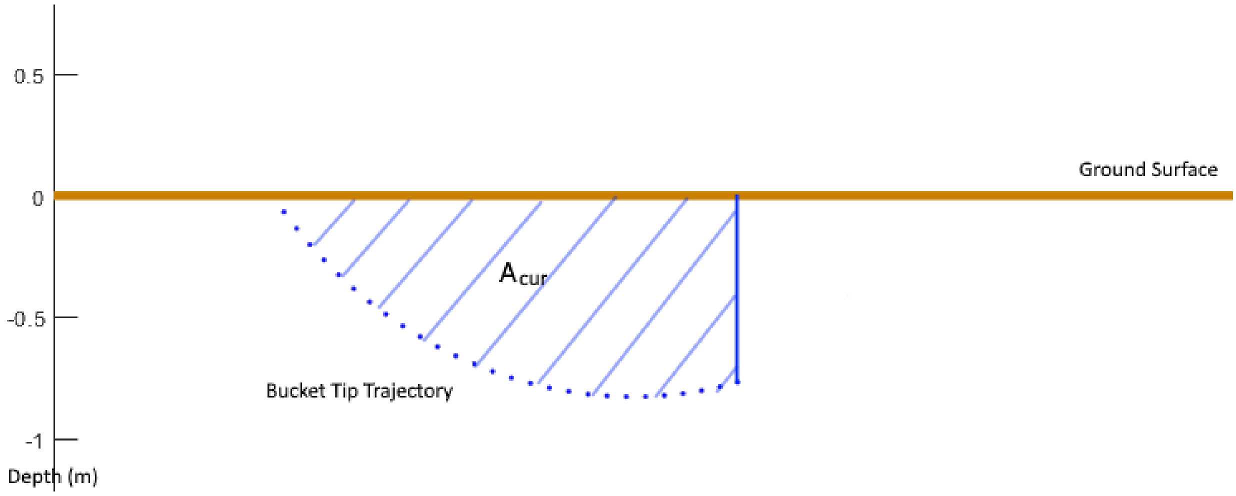

Figure 3.9. Area between the bucket tip trajectory and the ground surface

$$B_{fill}(\%) = \frac{V_{cur}}{V_{cap}} * 100 \tag{3.12}$$

where V_{cur} is the current volume inside the bucket and V_{cap} is the capacity volume of the bucket.

For the vertical force reaction, bucket weight has the major contributon during the loading phase. Bucket weight is calculated from multiplication of current soil volume inside the bucket with unit weight of the soil (Eq. 3.13).

$$W_{bucket} = \gamma_{soil} * V_{cur} = \gamma_{soil} * (B_{fill} * V_{cap}) \qquad (3.13)$$

where B_{fill} is the current bucket fill percentage.

3.1.6. Water Effect

There are many studies about the reactions of soil to water. Although there are some research works which examine the undrained soil's behavior in static condition, there are not many studies investigating the undrained soil's reaction during the excavation process.

It is known that the pore water pressure (u), reduces the shear strength in granular materials by decreasing the effective confining stress. Therefore the formula to find the shear strength in cohesionless soils can be written as (Eq. 3.14).

$$\tau = \sigma' tan\phi' = (\sigma - u) tan\phi' \qquad (3.14)$$

where τ is the shear strength, σ' denotes effective normal stress, ϕ' stands for effective angle of friction, and u is the pore water pressure.

3.1.6.1. Excavation in Unsaturated Soils

Solving the behavior of soil-tool interaction for surficial soils with their non-linear behavior is a very challenging topic. A significant number of studies have been conducted to understand soil-tool interaction behavior, and some methods have been developed for over half a century (Cannon, 1999; Reece, 1964; Singh, 1995; Vahed et al., 2008). However, very few investigations of soil-tool interaction in unsaturated soil have been conducted. Even though most analyses are based on saturated soil mechanics principles, the majority of the earth land surface is composed of unsaturated soils. Moreover, excavations take place in the top layer of the soil, which is assumed to be unsaturated. Therefore, ignoring or not focusing on the water-related issues is not a good practice in reality. A considerable number of researchers have proved that prediction of resistive forces which have been calculated by conventional saturated soil mechanics methods can differ on the non-conservative side when dealing with unsaturated soils. Although the rest of the thesis represents equations for saturated soils and the simulation tool does not include them, calculation of key forces for the excavation in unsaturated soils are summarized in this part.

3.1.6.1.1. Soil Weight

One of the key forces acting on the excavator bucket during digging is the weight of the soil accumulated in the bucket. To obtain more accurate results (γ_{sat} is conservative), unsaturated unit weight should be used as the excavation process is in unsaturated regions mostly during the earthmoving process, instead of dry or saturated unit weight. As it was stated by Head (2006), soil's unit weight for the unsaturated case can be calculated using the following formulation;

$$\gamma = \frac{(G + S * e)\gamma_w}{1 + e} \tag{3.15}$$

where γ is unit weight, G is specific gravity of solid particles, S is degree of saturation, γ_w is unit weight of water (equals to 9807 N/m^3), and e is void ratio. Unit weight of soils can easily be obtained in any geotechnical laboratory. One can measure γ, G, w in the labratory, then calculate S and e using phase relations such as Eq. 3.15.

3.1.6.1.2. Shear Strength

Eq. 3.14 can be extended to include suction in the case of unsaturated soils. Bishop et al. (1960) advice to use following widely accepted approach which is called effective stress approach for unsaturated soils;

$$\tau = c' + [\sigma - u_a + \chi(u_a - u_w)]tan\phi' \tag{3.16}$$

where τ is the shear strength, c' is effective cohesion, ϕ' is effective angle of internal friction, σ is total stress, u_w is pore water pressure, u_a is pore air pressure, χ is a soil parameter depending on the degree of saturation, the soil type, the moisture hysteretic state and the stress conditions. The term $(u_a - u_w)$ is called matric suction, and it replaces pore pressure of classical soil mechanics as the stress parameter governing the behavior of unsaturated soils.

In unsaturated soils, the water pulls the particles of the soil closer, and shear strength increase occurs. Many attempts have been made to determine χ value theoretically or empirically. Majority of these studies established a relation between χ and the degree of saturation. Coleman (1962) found out that the χ parameter is related to soil structure as well. Some other researchers tried to relate χ with capillary models, but they have failed. Khalili and Khabbaz (1998) proposed an accurate relationship, presented in

Figure 3.10, between χ value and the ratio of suction over the air entry suction value which can be extracted from soil water characteristic curve (SWCC) of the soil (Figure 3.11).

$$\chi = \left[\frac{\psi}{\psi_b}\right]^{-0.55} \qquad (3.17)$$

where ψ = matric suction and ψ_b = air entry suction.

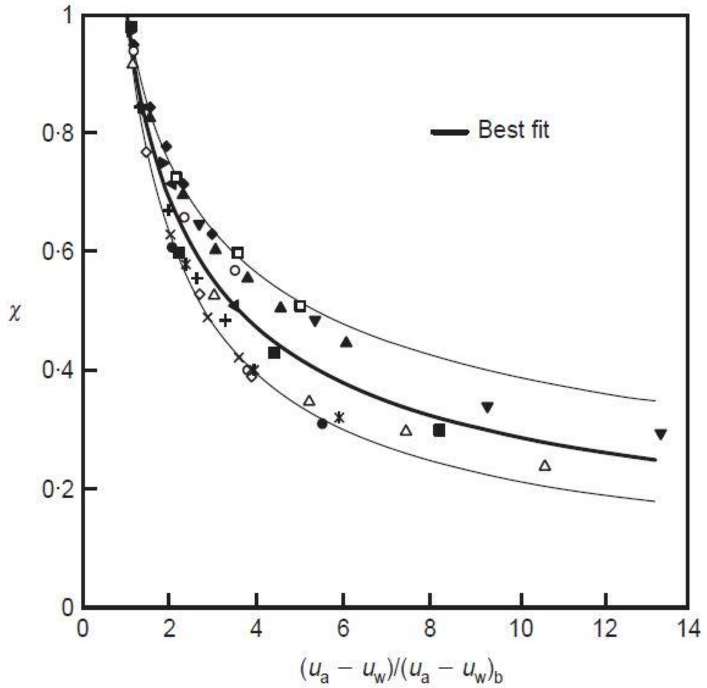

Figure 3.10. The relation between χ and the suction ratio (triangular, square and circle points are the experimental data points) (Khalili & Khabbaz, 1998)

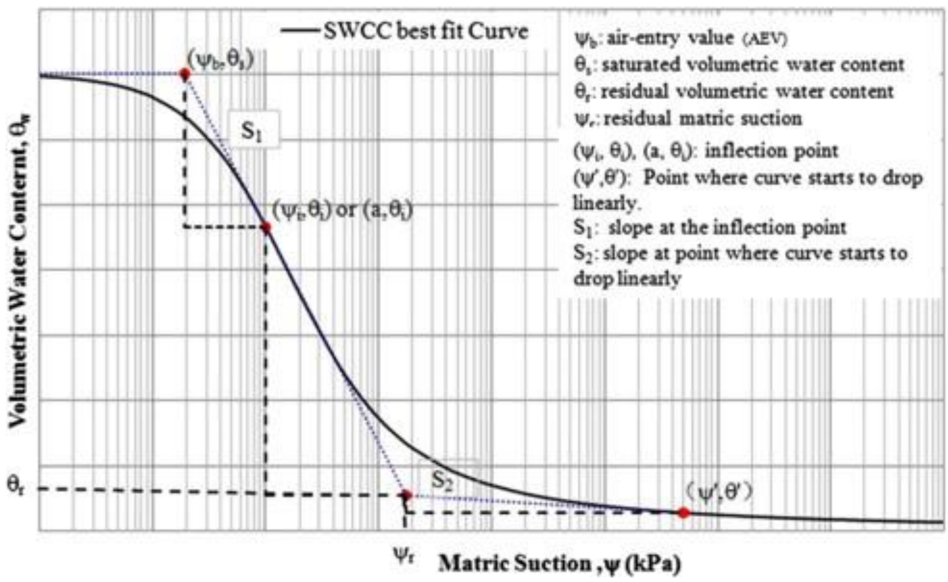

Figure 3.11. The soil-water characteristic curve with its parameters (Zhai & Rahardjo, 2012)

The shear strength equation for an unsaturated soil exhibits a smooth transition to the shear strength equation for a saturated soil. As the soil approaches saturation, the pore water pressure, u_w, approaches the pore-air pressure, u_a, and the matric suction, $(u_a - u_w)$, goes to zero. The matric suction component vanishes, and Eq. 3.16 transforms into the equation for a saturated soil.

Another version of the shear strength equation for unsaturated soils based on the independent state variables approach developed by Fredlund et al. (1978) represented in Eq. 3.18 and the failure envelope can be seen in Figure 3.12;

$$\tau = c' + (\sigma - u_a)tan\phi' + (u_a - u_w)tan\phi^b \qquad (3.18)$$

(where ϕ^b = angle of internal friction with respect to matric suction)

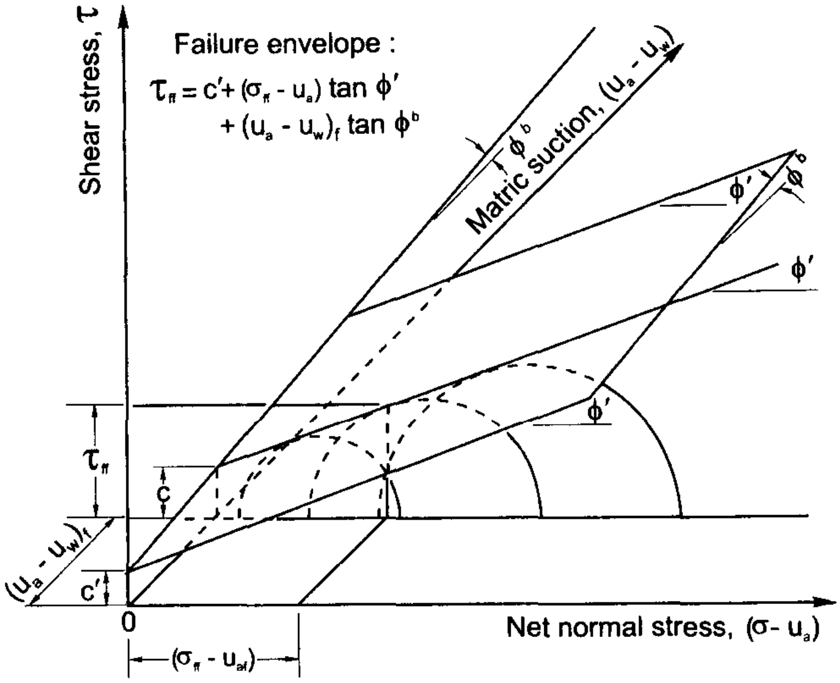

Figure 3.12. Mohr-Coulomb failure envelope for unsaturated soils (D. G. Fredlund & Rahardjo, 1993)

Although this approach has been widely promoted in the literature, it has very little application in practice. The main reason behind this situation is a requirement of extensive and time-consuming laboratory testing to find the material parameters, especially for fine-grained materials with a very low coefficient of permeability. Determination of ϕ^b needs expensive and sophisticated equipments that require a level of expertise to handle the experiment. For the time being, this is far beyond the traditional geotechnical laboratories.

Moreover, there is a limitation due to the high variability of ϕ^b vs. suction. Measurable suction range is limited to conditions where the suction range used in the laboratory to predict ϕ^b is the same as expected in the field (Khalili & Khabbaz, 1998). On the other hand, with the effective stress aproach (Eq. 3.16), the prediction of shear strength in unsaturated soils can be made without having sophisticated laboratory tests. The only different parameter used in the estimation of unsaturated shear strength is the air entry value other than saturated shear strength parameters, and this air entry parameter can be calculated relatively easily in any soil mechanics laboratory.

Some experimental studies have been made to have better understanding of the change in shear strength value concerning the change in matric suction or degree of saturation. Escario and Sáez (1986) shared their results on shear strength change concerning suction with different normal stress values (Figure 3.13). Fredlund et al., (1989) study concluded that the relationship between shear strength and matric suction is somehow non-linear as can be seen in Figure 3.14.

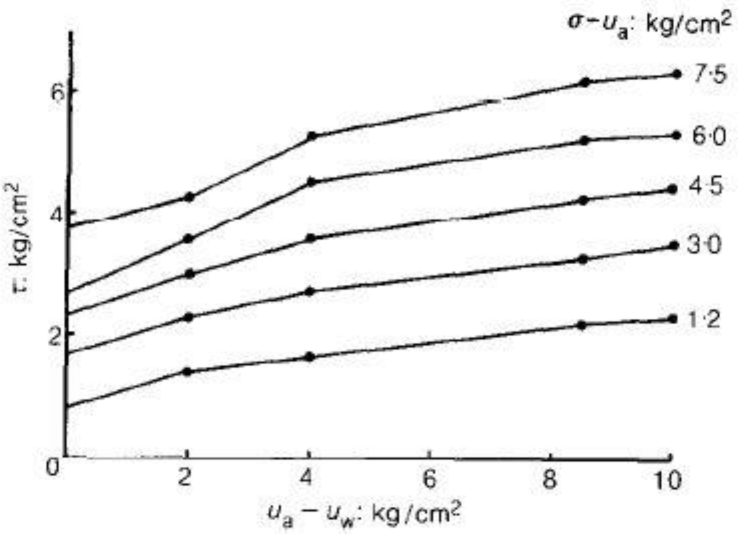

Figure 3.13. Shear strength vs. suction for different normal stress values (Escario & Sáez, 1986)

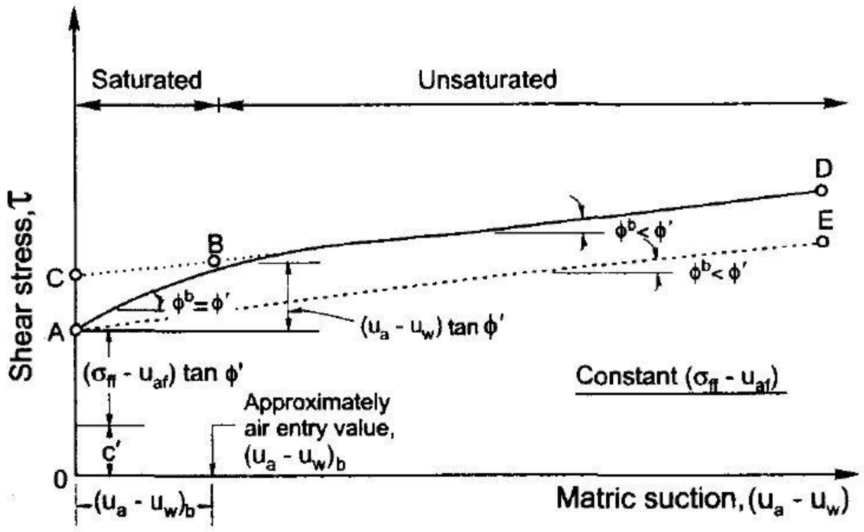

Figure 3.14. Non-linearity in shear strength vs. Suction (Fredlund et al., 1989)

3.1.6.1.3. Lateral Earth Pressure

For saturated soil mechanics, all stresses in Eq. 3.33.3 are effective stresses in a drained analysis. This can also be done for unsaturated soils if effective stress approach (ESA) is used. Alternatively, in the case of independent state variables approach (ISVA) (Figure 3.15, Eq. 3.18), as well as with ESA, the effect of suction can be converted into an increase in total cohesion (c) as Eq. 3.19 and Eq. 3.20, and use Eq.3.3 3.3 with total stresses.

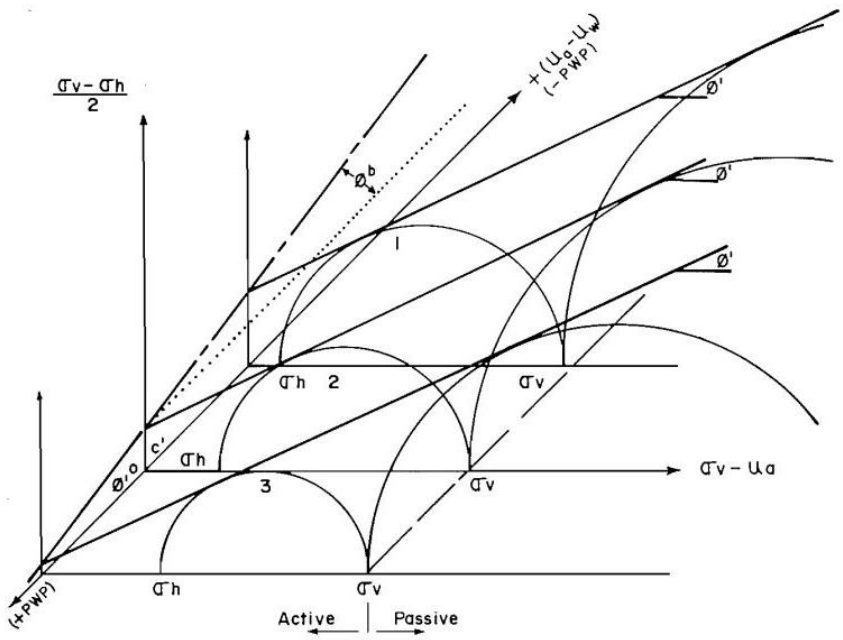

Figure 3.15. Active and passive earth pressure for saturated and unsaturated soils (Fredlund & Rahardjo, 1993)

ESA: $$c = c' + (u_a - u_w)\chi tan\phi' \qquad (3.19)$$

ISVA: $$c = c' + (u_a - u_w)tan\varphi^b \qquad (3.20)$$

It is possible to select various distributions for matric suction with respect to depth. As we deal with the very top of the soil section which is contacts with air, in this study matric suction was selected to be linearly decreasing with depth until it becomes zero at the water table. The equation can define any matric suction distribution;

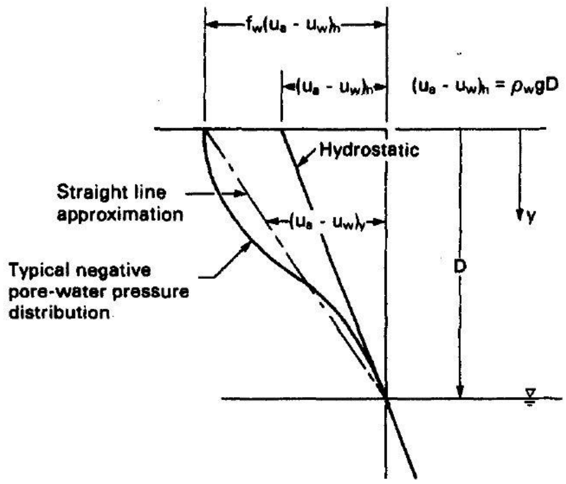

Figure 3.16. Matric suction profile (Fredlund & Rahardjo, 1993)

$$(u_a - u_w)_y = f_w(u_a - u_w)_h(1 - \frac{y}{D}) \qquad (3.21)$$

Then, passive pressure can be written as below;

$$\sigma_p = (\sigma_v - u_a)K_p + 2c'\sqrt{K_p} + \ 2f_w(u_a - u_w)_h tan\varphi^b(1 - \frac{y}{D})\sqrt{K_p} \qquad (3.22)$$

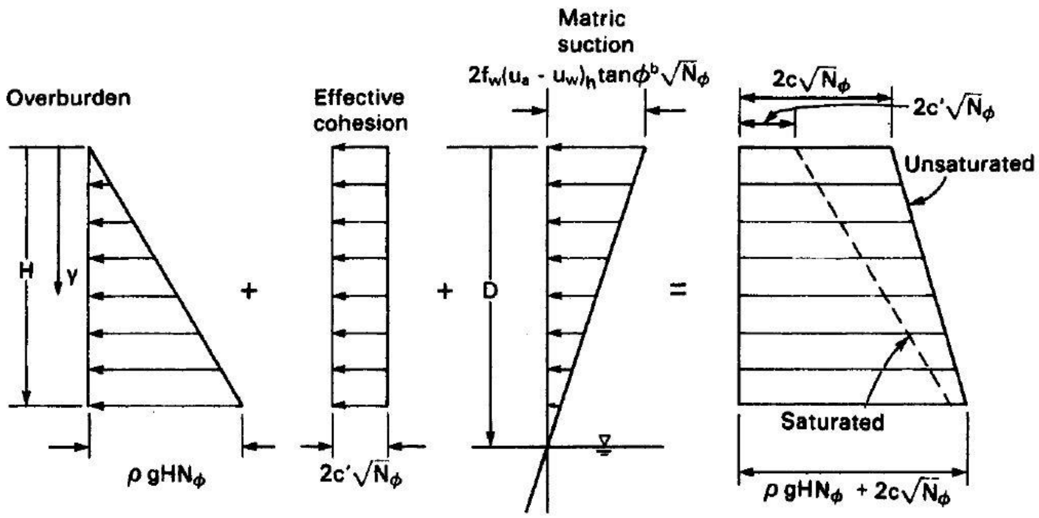

Figure 3.17. Passive pressure where matric suction is decreasing linearly with depth (Fredlund & Rahardjo, 1993)

To obtain total horizontal earth pressure integration of Eq. 3.22 over depth is required. Then total passive pressure equation for unsaturated soils become (Pufahl et al., 1983);

$$\boldsymbol{P}_p = \frac{\rho g N_\varphi H^2}{2} + 2c'\sqrt{K_p}H + 2f_w(u_a - u_w)_h tan\varphi^b\sqrt{K_p}(H - \frac{H^2}{2D}) \quad (3.23)$$

3.1.6.1.4. Tip Resistance

The formulation provided in Section 3.1.4 was developed for saturated soils. Using the same formulas for unsaturated soils may lead to misrepresentations in estimating force. Besides, some experimental studies revealed that the effects of suction may cause the tip resistance to be doubled (Russell & Khalili, 2006). Therefore, neglecting this influence is not logical. For the calculation of tip resistance in unsaturated soils, the effective stress defined in Section 3.1.6.1.2 should be used.

There are constant and linearly decreasing approaches for the suction distribution, as mentioned in Section 3.1.6.1.3. For the cavity expansion theory, Russell and Khalili (2006b) stated that there is no considerable difference between these two distributions. Therefore, the formula (Eq. 3.24) has been constructed for constant suction distribution. However, as there is not much difference, they can also be used for linearly decreasing distribution case.

An empirical equation (Eq. 3.24) for cavity expansion pressure has been developed using a reasonable fit to results of tests on sand. represents constant suction spherical cavity expansion results in the p_0 (initial total cavity pressure) – σ_{rlim} (net limiting radial stress) plane for different values of χs or $\chi\psi$ and D_r.

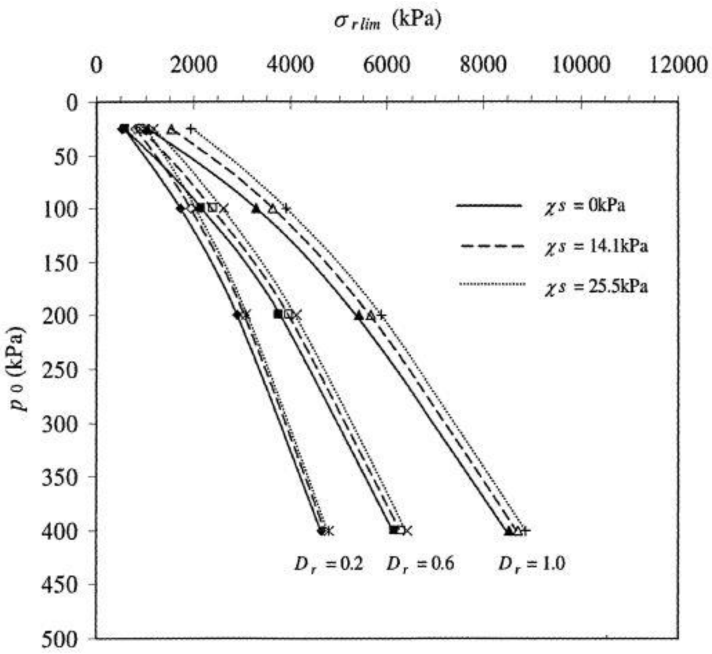

Figure 3.18. Spherical cavity expansion results for drained conditions and a range of D_r and χs values (Russell, 2004)

$$\sigma'_{rlim} = (16.3 - 18.6 ln D_r) {p'_0}^{0.7} \exp(2.1 D_r) \qquad (3.24)$$

Change in suction stresses do not affect net limiting radial stress dramatically unlike D_r. Therefore, the formula has only parameters D_r and p'_0. Eq. 3.24 can be used instead of Eq. 3.8 for the unsaturated soils to predict tip resistance of the excavator bucket while digging.

For shallow depths, which is mostly the case for excavation, tip resistance can be more than double concerning their saturated or dry values when saturation ratio is less than 0.1 as can be seen in Figure 3.19.

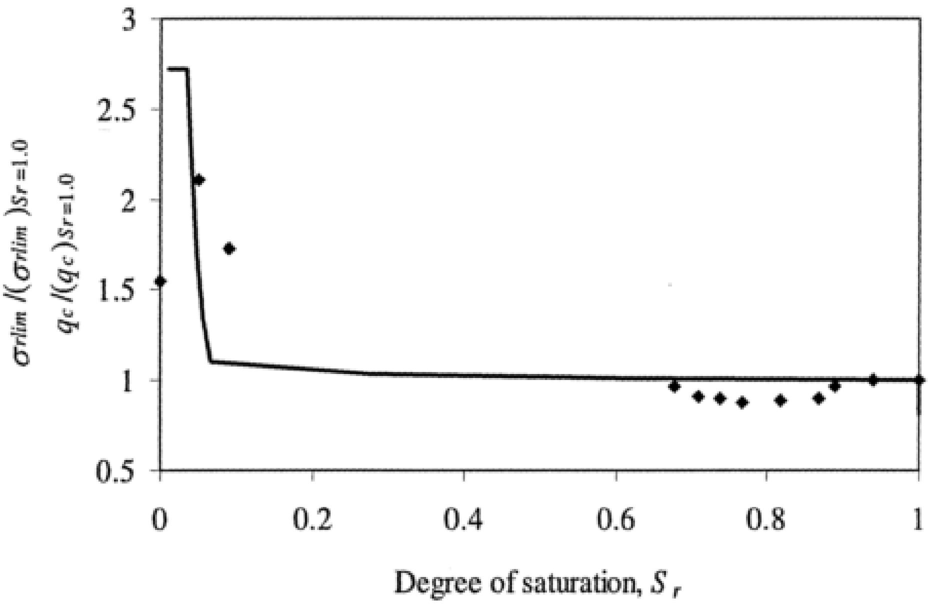

Figure 3.19. Comparison of cone penetration test results with spherical cavity expansion results (Russell & Khalili, 2006)

3.1.7. Velocity Effect

The dynamic effects in the excavation process are examined by conducting experiments and making predictions using related formulas. According to McKyes (1985), the effect of the velocity differs with soil type. Unlike in cohesive soils, in cohesionless soils, shear rate does not have a significant impact on the strength of the material. These types of soils are affected by the inertial forces that can be calculated by considering the influence of the acceleration. However, in cohesive materials, the shear strength depends on the shear rate and not on the inertial forces that are affected by the changes in the velocity.

Wheeler & Godwin (1996) used an experimental setup to understand velocity effect for the earth-moving related problem, and compared the results of the experiments to the predicted data. These experiments are conducted for the frictional and cohesive soils, and the velocity range used in the experiments is varied from 1 to 20 km/h. The results of these experiments and comparisons between the results and the predicted data in graphical form can be seen in Figure 3.20 and Figure 3.21.

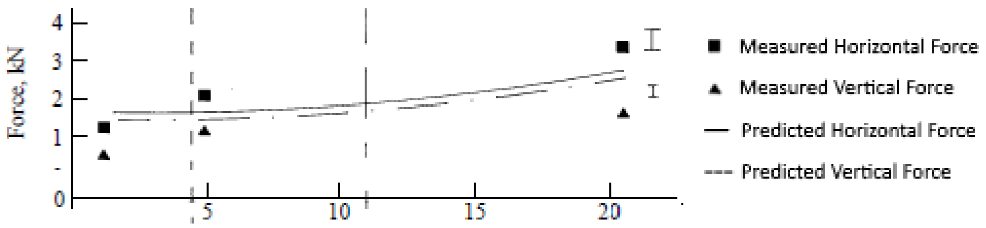

Figure 3.20. Force vs. velocity graph for frictional soils (Wheeler & Godwin, 1996)

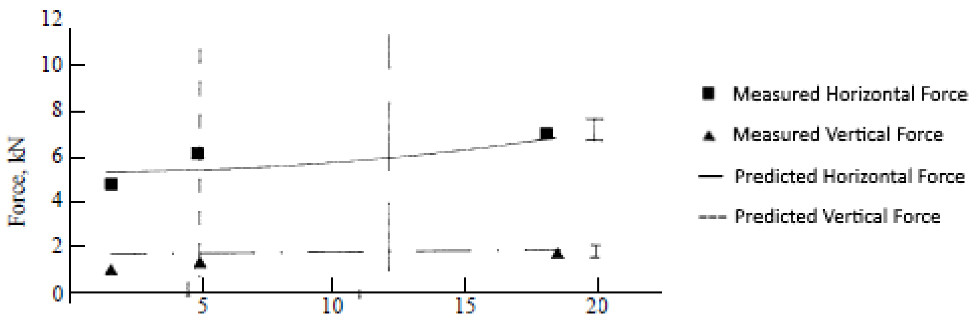

Figure 3.21. Force vs. velocity graph for cohesive soils (Wheeler & Godwin, 1996)

It can be seen that the increase in velocity affects the horizontal force with a small amount, in both frictional and cohesive soils. However, in the case of vertical force, the frictional soil has a more dramatic change than the cohesive soil with the increasing velocity.

Qinsen and Shuren (1994) came up with a conclusion saying that for low velocities, draft force acting on the tool surface is not significant, and as other studies supported, velocity becomes a significant parameter when its value is high as can be seen in Figure 3.22.

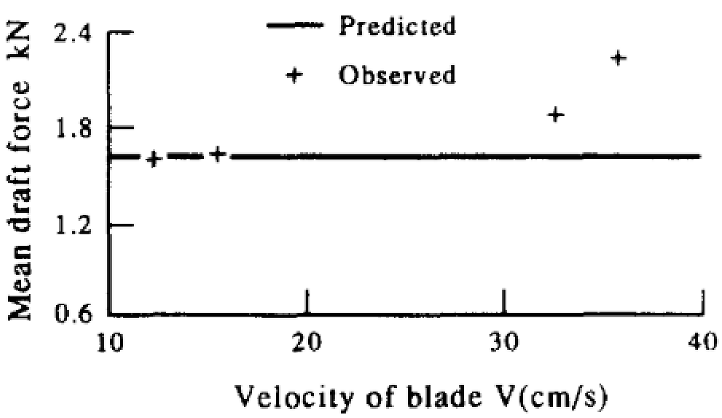

Figure 3.22. Resistive force vs. velocity for both experimental and predicted data with Qinsen & Shuren Model (Qinsen & Shuren, 1994)

Abo-Elnor et al. (2003) investigated the impact of the velocity and acceleration on blade cutting forces using finite element methods. The forces of sandy soil in the horizontal direction were observed at constant velocities of 10, 30, 50, 100, 200 mm/s by running different models of finite element. Results are presented in Figure 3.23.

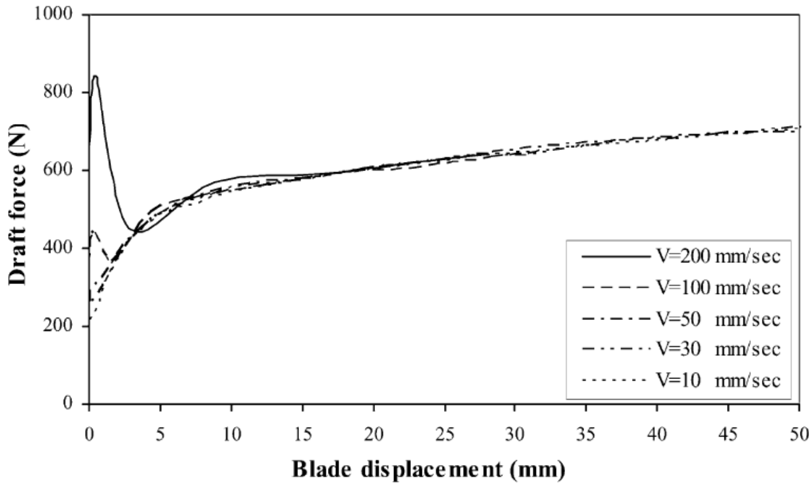

Figure 3.23. Draft force vs. blade displacement at different constant velocities (Abo-Elnor et al., 2003)

It is observed that the velocity introduced to a soil at-rest increases the draft force initially, but as the blade moves through the soil, this effect vanishes. Therefore, it can be said that the draft force is affected by the acceleration, and constant velocity does not have an impact on the draft force.

In the light of the previous studies, it is found appropriate to assume that soil reaction due to speed increase is insignificant for the scope of earthmoving machines and therefore simulation tool does not consider the effect of velocity. Nevertheless, it should be considered that experimental studies show that excavation force is a function of velocity ($F = \beta_0 + \beta_1 * v + \beta_3 * v^2$ where β values are regression coefficients and v is velocity) (Onwualu, 1998).

3.2. Visualization

3.2.1. Failure Plane

During the digging process, it is assumed that the soil shows passive lateral resistance. Terzaghi (1943) provided a solution for defining the failure plane, which is called the log-spiral method where the failure plane has a logarithmic spiral shape, and moments and forces are calculated accordingly. McKyes (1985) advises to use this for the shape of excavation failure plane.

Figure 3.24 shows the general shape of the failure line for passive soil failure. For each ξ line, like |AD|, θ remains the same between the boundaries and in the region ABC. ξ lines are straight and make 2μ angle at the intersection with a η line, like |BC|.

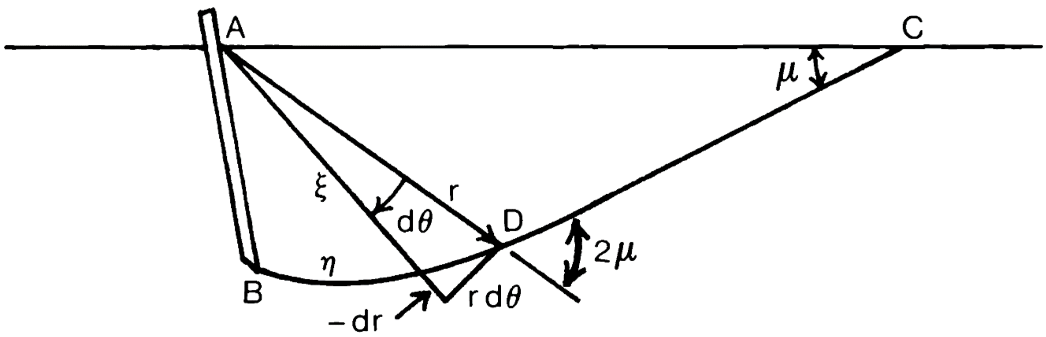

Figure 3.24. Characteristic failure surface shape (McKyes, 1985)

Using geometry on the small triangle which has sides *-dr* and $rd\theta$, this relationship is calculated using Eq. 3.25,

$$-dr = rd\theta cot2\mu = rd\theta tan\phi$$

$$r = C_3 e^{-\theta tan\phi} \tag{3.25}$$

where C_3 is a constant of integration that can be evaluated at a boundary.

To investigate the soil cutting problem using vertical rigid walls' movement in the soil and to further validate the Terzaghi's approach, Maciejewski et al. (2003) used an experimental setup in the laboratory, of which experimental details are shown in Figure 3.25. The bin dimensions were 2m long, 0.6m wide and 1.2m deep. The soil used in the experiment has γ = 16.8 kN/m^3, φ = 27°, c = 30 kPa. The test equipment had the capability of moving 400mm horizontally and 100mm vertically into the soil. A failure plane was obtained as shown with a red line in Figure 3.26. Failure line was identified with the help of image processing techniques. Figure 3.27 reveals the comparison of the experimental failure plane with the log-spiral failure plane, indicating that there is a very good agreement. To date, the log-spiral method has been the best method in the literature to explain failure plane generated during the digging process.

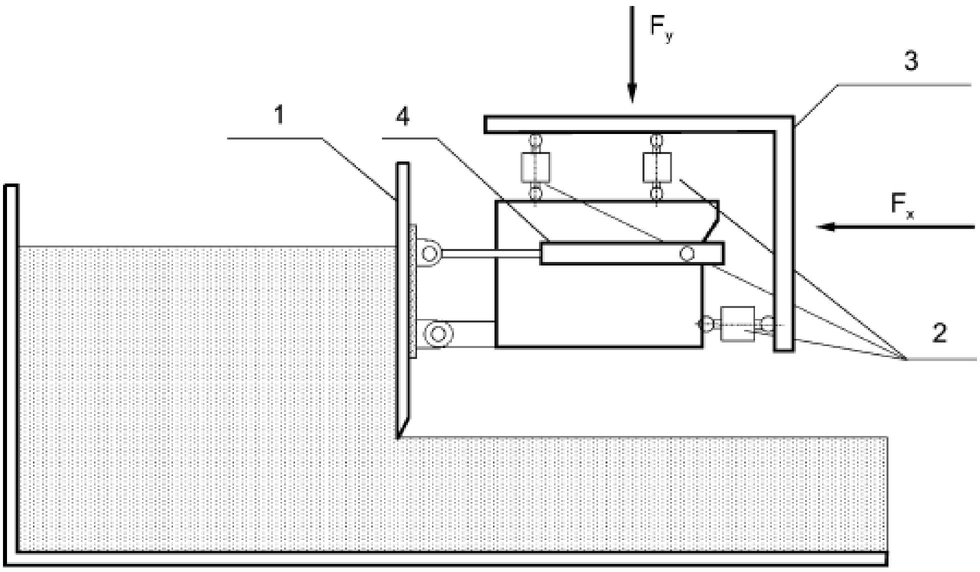

Figure 3.25. Experimental setup: (1) vertical plate; (2) load cells; (3) rigid frame; (4) hydraulic cylinders (horizontal, vertical and rotational) (Maciejewski et al., 2003)

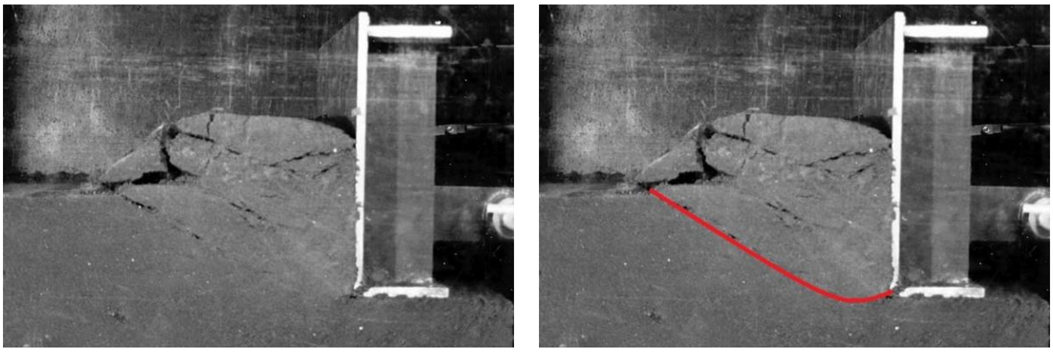

Figure 3.26. Failure plane

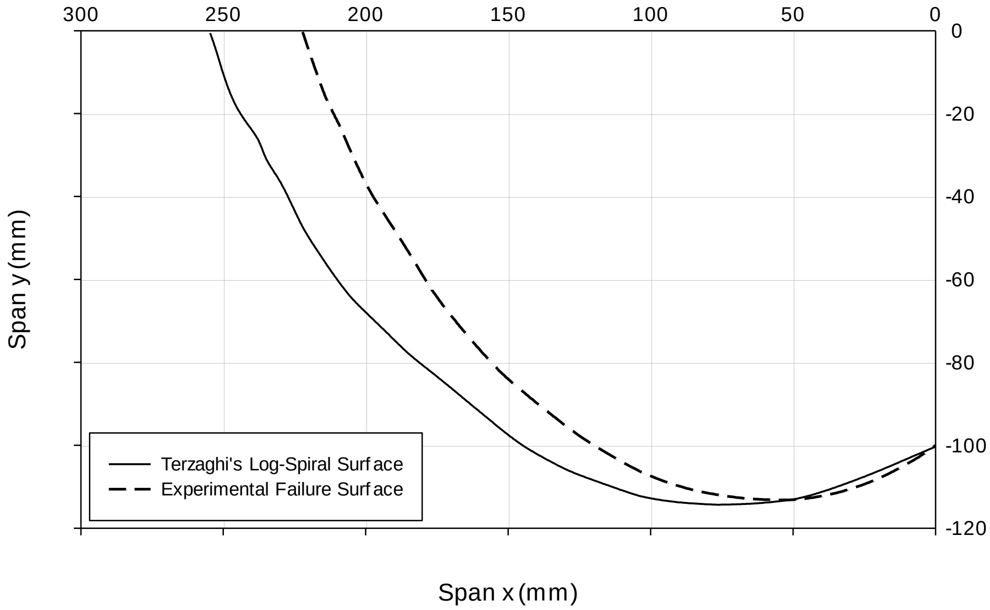

Figure 3.27. Comparison between Log-Spiral and Experimental Failure Planes

3.2.2. Bucket Capacity

Bucket capacity is the maximum volumetric measurement of the material that bucket of the backhoe excavator can store. It can be calculated in two different ways, which are (i) struck capacity, and (ii) heaped capacity. Struck capacity is the capacity that the bucket is filled until the struck plane, which is represented in Figure 3.28. Heaped capacity is defined as the summation of the struck capacity and the capacity of the excess material that is heaped on the struck plane. There are two global calculation methods to determine heaped capacity. These methods are listed as, SAE J296: "Mini excavator and backhoe bucket volumetric rating", an American standard, (SAE Internationals, 1999) and, CECE (Committee of European Construction Equipment), a European standard (Gaurav, 2008). According to the SAE J296, excessed material heaped on the struck plane is at 1:1 angle of repose, while that of one is at 2:1 according to the CECE.

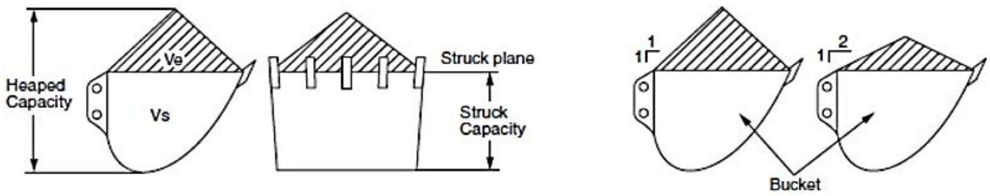

Figure 3.28. Bucket struck and heaped capacities (Park, 2002)

The heaped capacity is given in Eq. 3.26,

$$V_h = V_s + V_e \tag{3.26}$$

where V_h is the heaped capacity, V_s is the struck capacity, and V_e is the excess material capacity.

Dimensions of the bucket and heaped material are given in Figure 3.29.

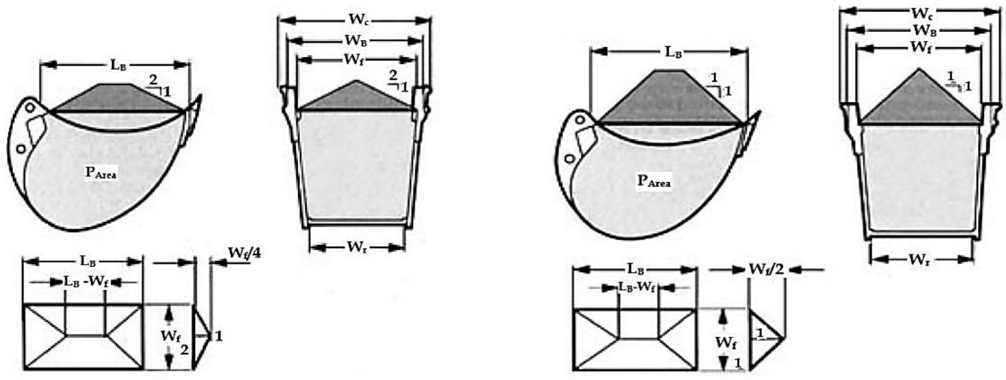

(a) (b)

Figure 3.29. Bucket capacity rating (a) according to CECE (b) according to SAE (Gaurav, 2008)

Then, the struck capacity and excess material capacity are formulated in the Equations 3.27 to 3.29 for Struck Capacity, Excessed Material Capacity (V_e) according to SAE J296 standard, and Excess Material Capacity (V_e) according to CECE standard, respectively. In this research, the value of maximum bucket capacity provided in the manual of the simulated bucket was utilized.

Struck Capacity (V_s):

$$V_s = P_{area}\left(\frac{(W_f + W_r)}{2}\right) \tag{3.27}$$

- Excess Material Capacity (V_e) according to SAE J296 standard:

$$V_e = \left(\frac{L_b {W_f}^2}{4} - \frac{{W_f}^3}{12}\right) \tag{3.28}$$

- Excess Material Capacity (V_e) according to CECE standard:

$$V_e = \left(\frac{L_b {W_f}^2}{8} - \frac{{W_f}^3}{24}\right) \qquad (3.29)$$

In the field, it is observed that different soil types give different bucket fill reaction during digging process. In the clayey (cohesive) and stiff domain, heap height generated in the bucket is higher than the sandy (cohesionless) and loose domain. Water inclusion has also an important effect on the heap height generated over the bucket. If the digging is made on the saturated sand, the heap height is less than the dry case. On the other hand, during the digging in the saturated clay domain, heap height is higher than the dry case.

These effects should be included both in the bucket capacity, bucket weight and visualization calculations.

3.2.3. Unloading of Bucket

It is accepted that the amount of soil in the excavator bucket will linearly decrease during unloading as shown in (Kim et al., 2013). This approximation is validated by field observations made by the authors (Figure 3.31). Unloaded soil will create a heap with slope on its sides equal to the angle of repose.

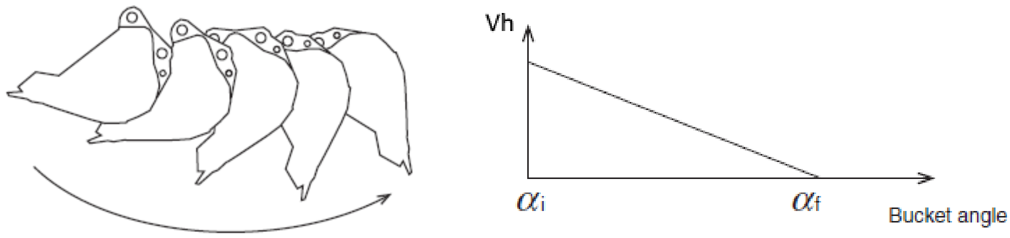

Figure 3.30. Linear decrease on volume during unloading (Kim et al., 2013)

Figure 3.31. Field observation for unloading

The angle of repose value is related to the internal friction angle of soils. Ghazavi, Hosseini, & Mollanouri (2008) provides a formula to obtain the angle of repose from the angle of friction given in Eq. 3.30.

$$\theta = 0.36\phi + 21.2\ (in\ degree) \quad (3.30)$$

During dumping, the volume of the soil inside the bucket (V_h) decreases linearly as a function of bucket angle (α). It is assumed that soil creates a heap with width greater than or equal to the bucket's width, and side angles equal to the angle of repose, like the examples given in Figure 3.32.

The simulation tool, developed within the scope of the thesis, does not have the unloading phase of the excavation process. However, research and comments on this subject provided to give idea for future studies.

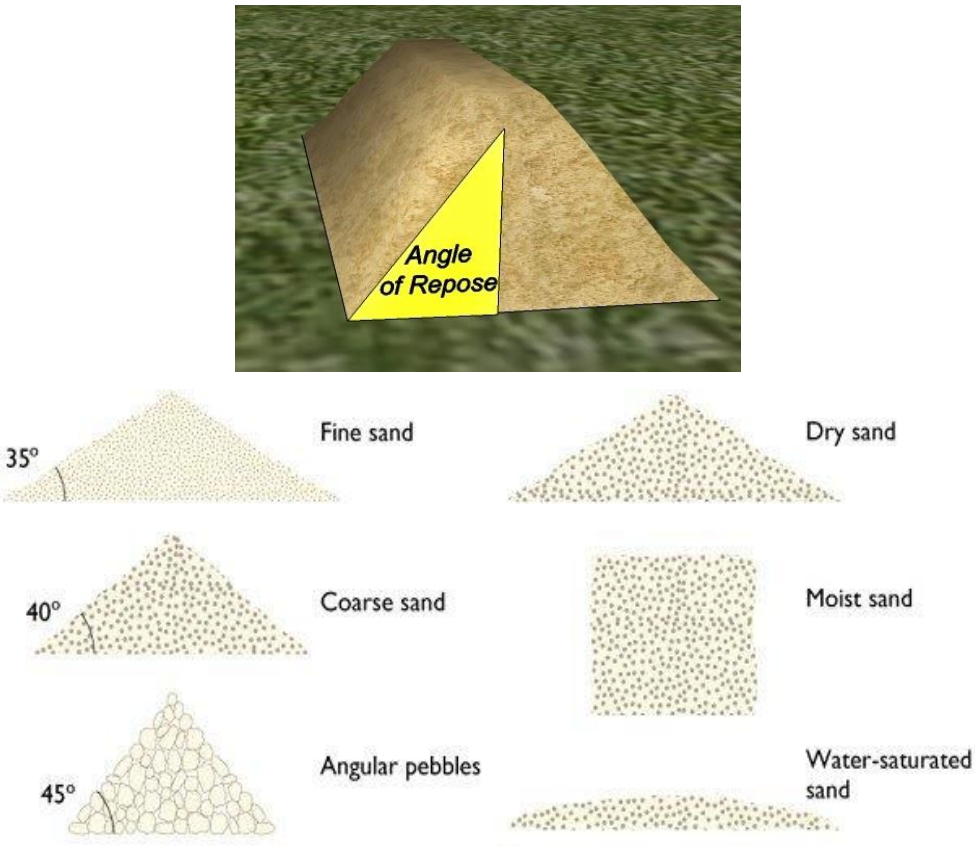

Figure 3.32. Heaps formed with an angle of repose (Buildsum, 2014)

CHAPTER 4

SIMULATION TOOL AND RESULTS

This chapter presents the software form of the equations presented in Chapter 3 that belongs to the stages of the excavation. To use the software in a friendly way and to be used in a simulator, a graphical user interface (GUI) is also provided here. With the complete framework, the results are obtained for illustrative case studies to outline the success of the simulation of the excavator. To validate the outcomes, results obtained from the literature studies are used. It is important to highlight that simulation tool, which is designed for validation of the proposed method, does not cover all titles mentioned in the Section 3. Simulation algorithm flow (Figure 4.1) shows the related sections used to develop the tool.

4.1. Modelling and Simulation Tool

The flowchart of soil tool model, the fundamentals of which was explained in Chapter 3, is prepared and coded within the MATLAB environment as an excavator-soil interaction platform. This platform takes all the inputs including the bucket geometry, the type of soil and the state of ground water table, etc., at the beginning. The flowchart of the software, which calculates the forces, corresponding movements of the bucket and the overall motion commands at every frame is given in Figure 4.1.

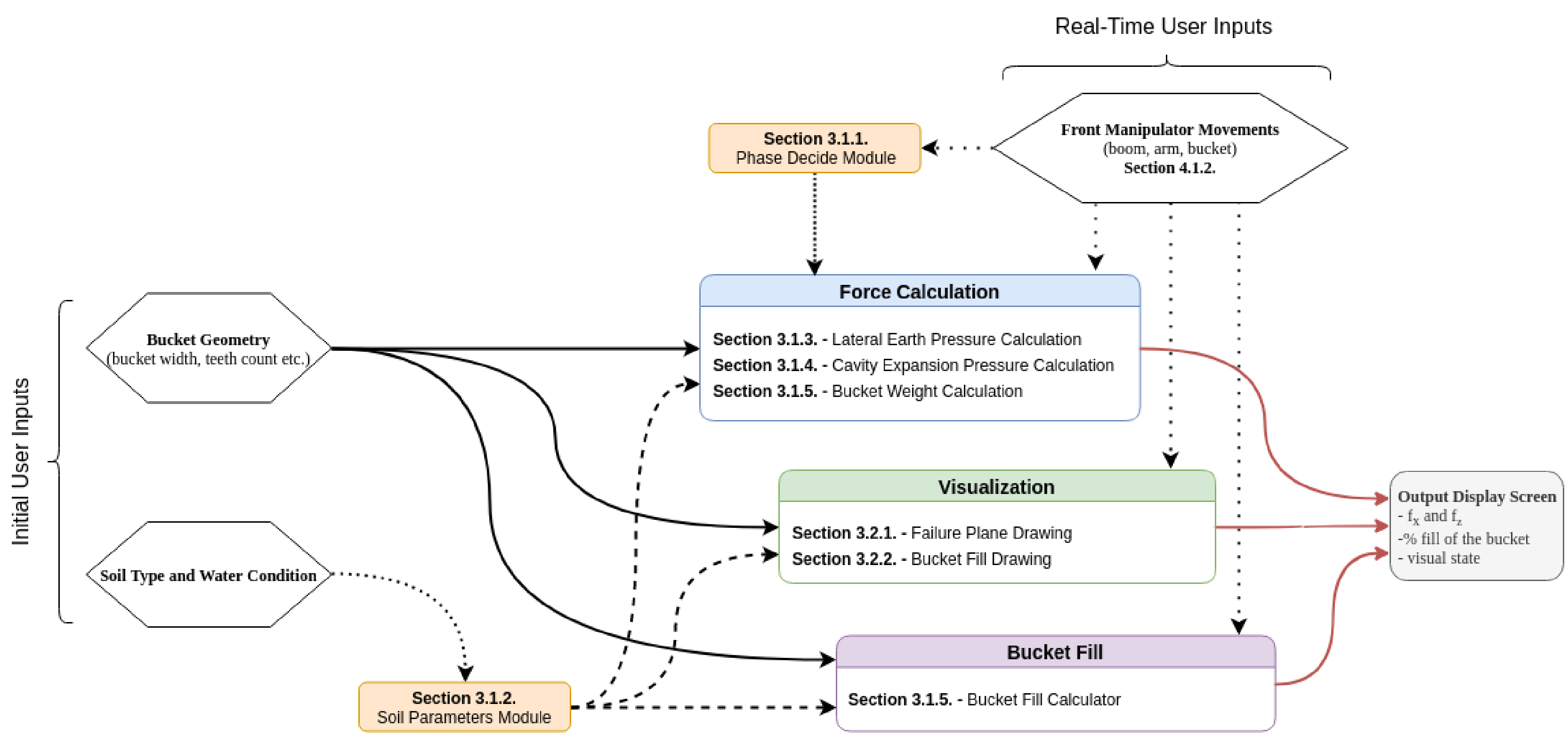

Figure 4.1. Simulation algolrithm flow

4.1.1. MATLAB/GUI

MATLAB software has been chosen to develop soil-tool interaction algorithm, because exploring data, creating algorithms, and visualization in 2-D are easy with MATLAB's open architecture which provides early insights and numerous advantages (Dukkipati, 2010). Algorithms developed with MATLAB can easily be shared with other researchers thanks to its open and transparent architecture (Leite, 2010). The algorithms have been implemented on the main body of MATLAB code, and GUI is provided to get user inputs such as bucket geometry and soil type. Excavator tool-soil interaction simulations have been performed in two-dimensional scale. Forces acting on the excavator bucket in horizontal and vertical directions have been recorded in every frame. Moreover, real-time simulation with results is displayed on GUI. The produced GUI uses joystick inputs to control boom, arm and bucket movements for real-time simulation. A sample model of digging process is displayed in Figure 4.2.

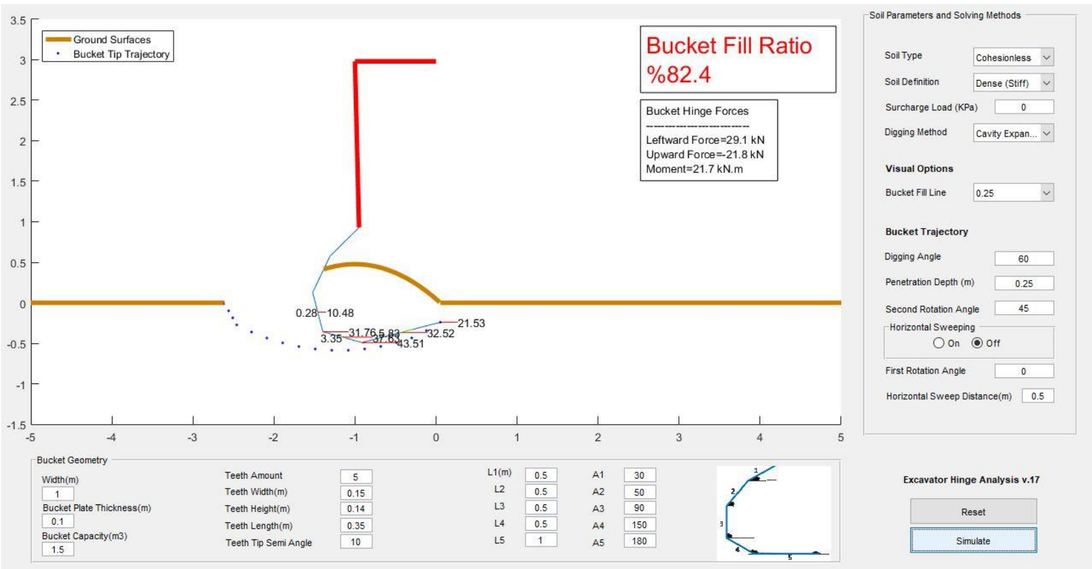

Figure 4.2. Sample screenshot from GUI

4.1.2. Joystick Input

It is aimed to have a real-time simulation in this research. Joystick or keyboard inputs can be used for controlling an excavator in real-time simulation. With the help of a controller device, users can control the boom, arm, and bucket movements of an excavator. Bodson (2003) provides a way to give inputs to the MATLAB environment using a joystick. As this thesis provides a real-time simulation on MATLAB, the controller enables the user to gain an appreciation for challenges of control. Manual control with a joystick is an excellent opportunity to have a better insight for both understanding soil behavior and control of the excavator itself. Figure 4.3 provides a sample screenshot of excavation control through joystick.

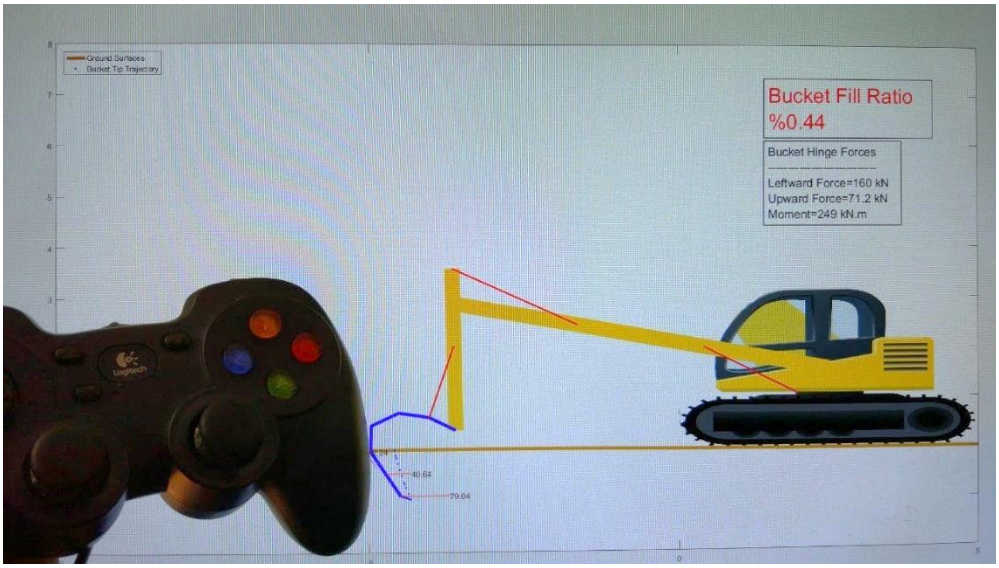

Figure 4.3. Controlling a simulated excavation operation through a joystick

4.2. Simulation Results

The results of the simulation studies, i.e., the vertical and horizontal resistive forces acting on the bucket are presented for different scenarios, along with the defined trajectory displayed in Figure 4.4, are given from Figure 4.8 to Figure 4.16. This trajectory is obtained through digging the soil at an angle of 80° and two different rotations of the bucket that brings its flat part to angles of 0° and -60° with the horizontal plane (Figure 4.5). The bucket moves with a constant time steps. Soil parameters used for each soil type listed in Section 3.1.2, which are dry and saturated forms of both cohesionless and cohesive soils. The relative density of sands changed from very loose to very dense, while consistency of clays varied from very soft to very stiff. The bucket geometry and bucket tip dimensions can be seen in Figure 4.6 and Figure 4.7, respectively. It is important to note that the bucket width has been selected as 1 m. The cutting force is the resultant total force on the bucket hinge where positive horizontal component (f_x) is rightward and positive vertical component (f_z) is downward. The program can be adjusted for other bucket types, which is planned for future studies.

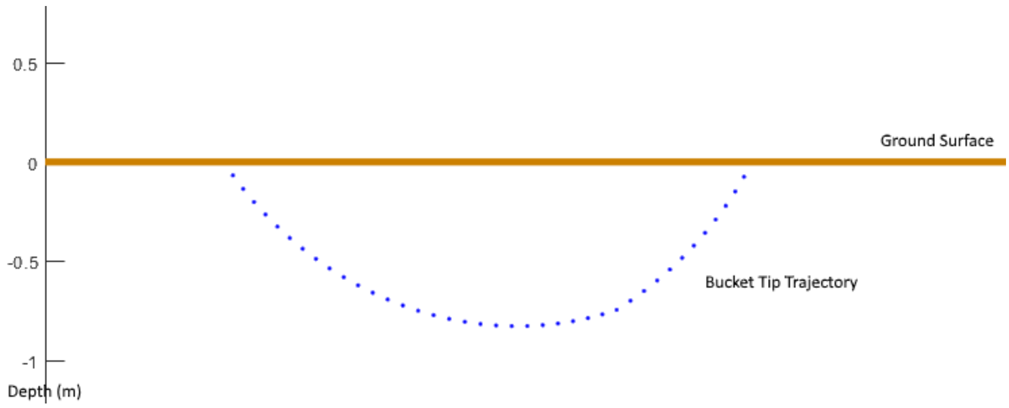

Figure 4.4. Bucket tip trajectory for simulated case

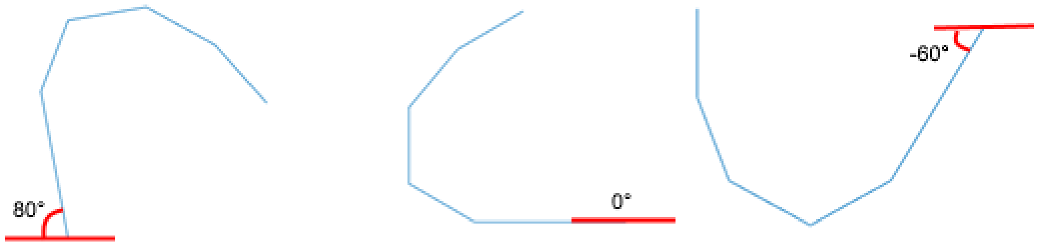

Figure 4.5. Digging and rotation of bucket to load soil into the bucket

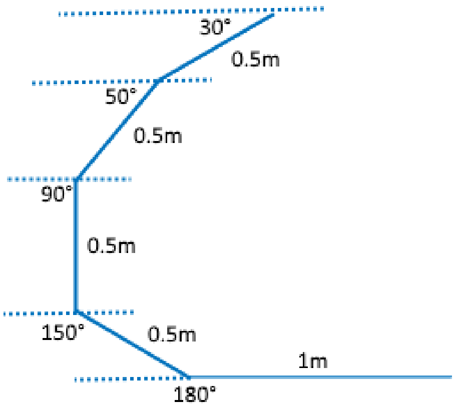

Figure 4.6. Bucket geometry (side view) for simulated case

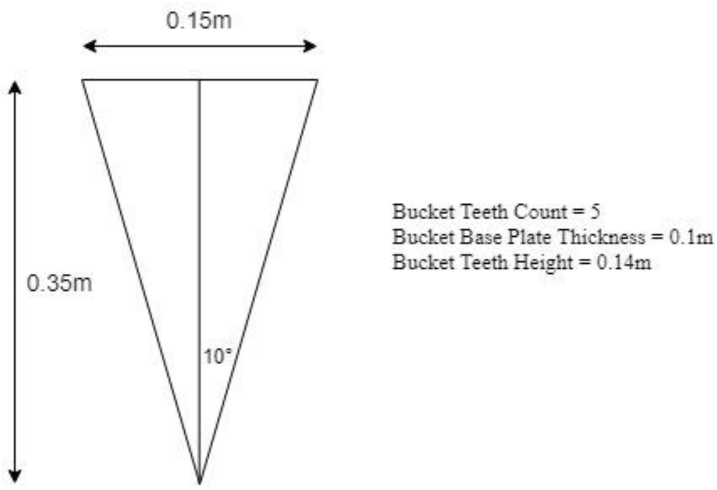

Figure 4.7. Bucket teeth geometry and details for simulated case

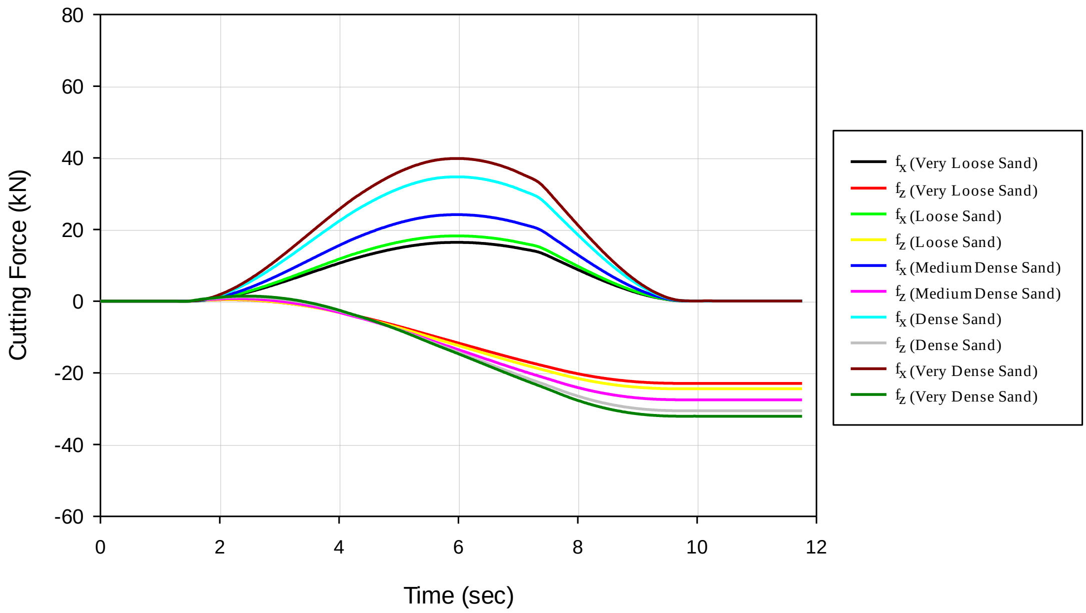

Figure 4.8. Simulated resistive forces for cohesionless dry soil

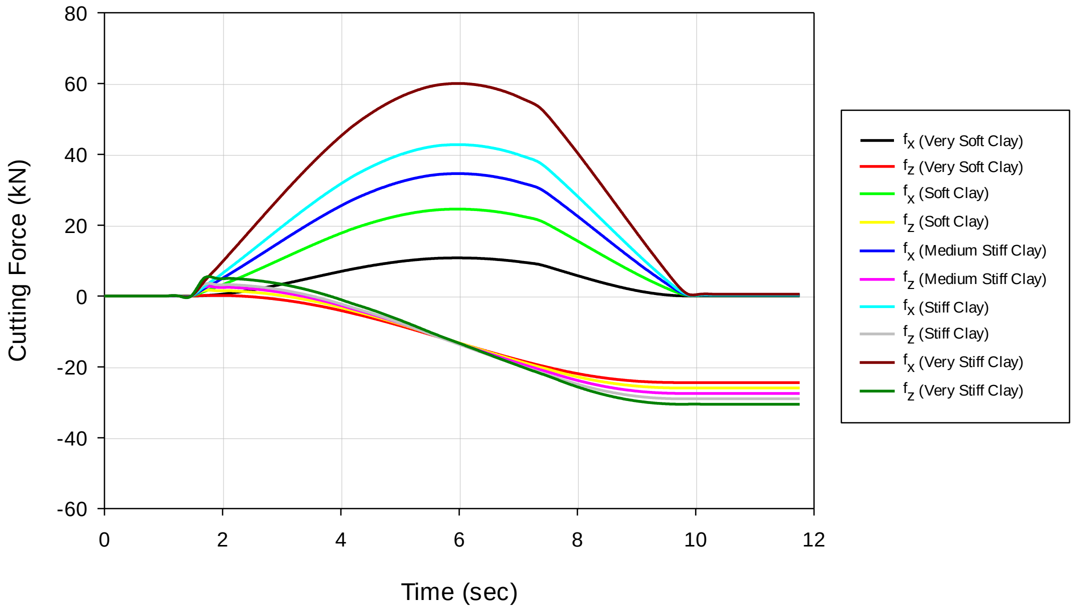

Figure 4.9. Simulated resistive forces for cohesive dry soil

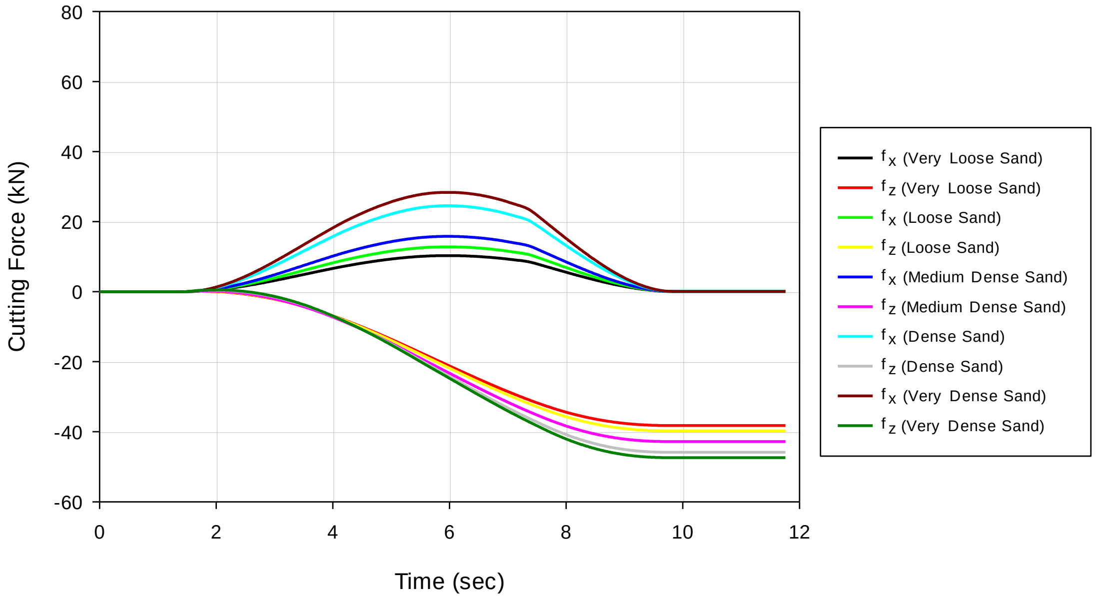

Figure 4.10. Simulated resistive forces for cohesionless saturated soil

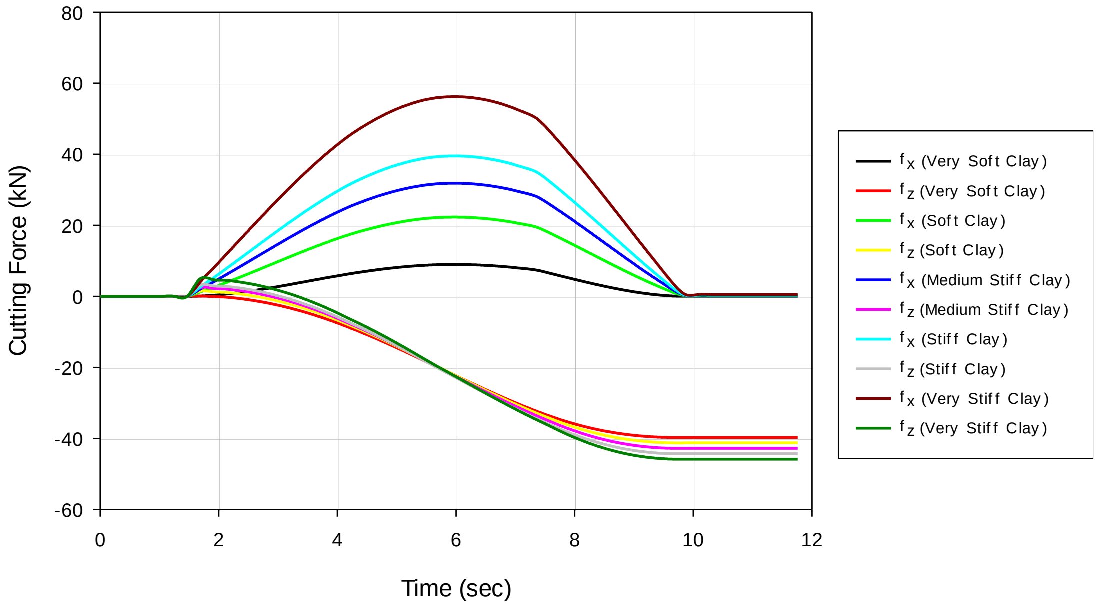

Figure 4.11. Simulated resistive forces for cohesive saturated soil

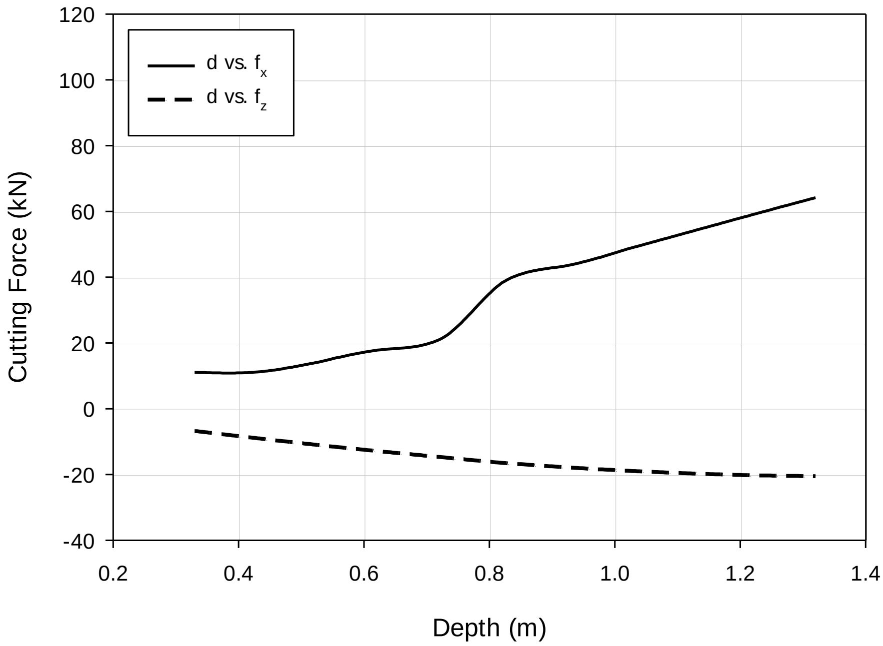

Figure 4.12. Simulated resistive forces for different cutting depths in medium stiff clayey soil

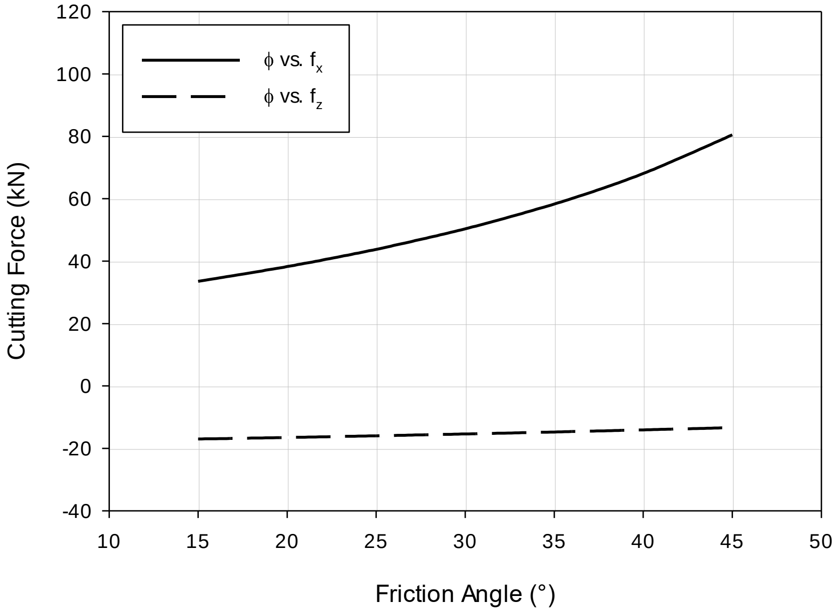

Figure 4.13. Simulated resistive forces for different friction angles

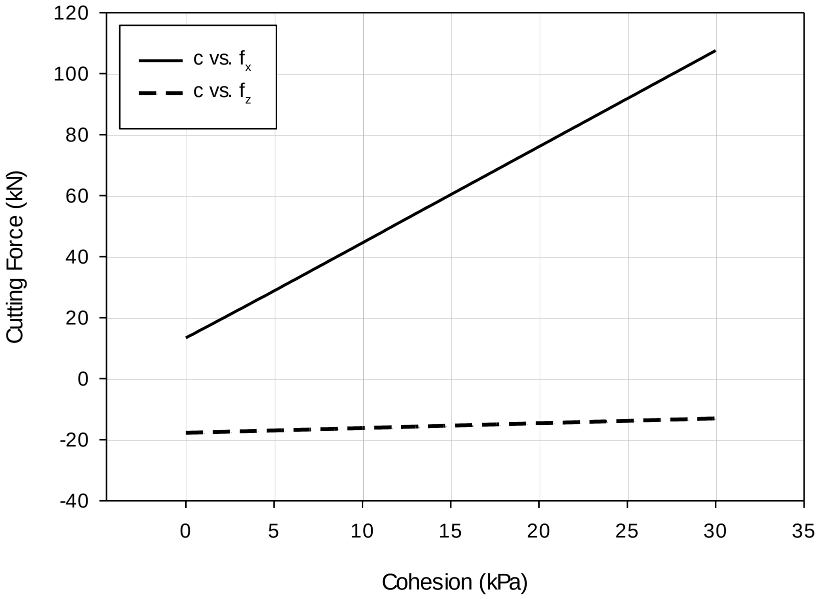

Figure 4.14. Simulated resistive forces for different cohesion level

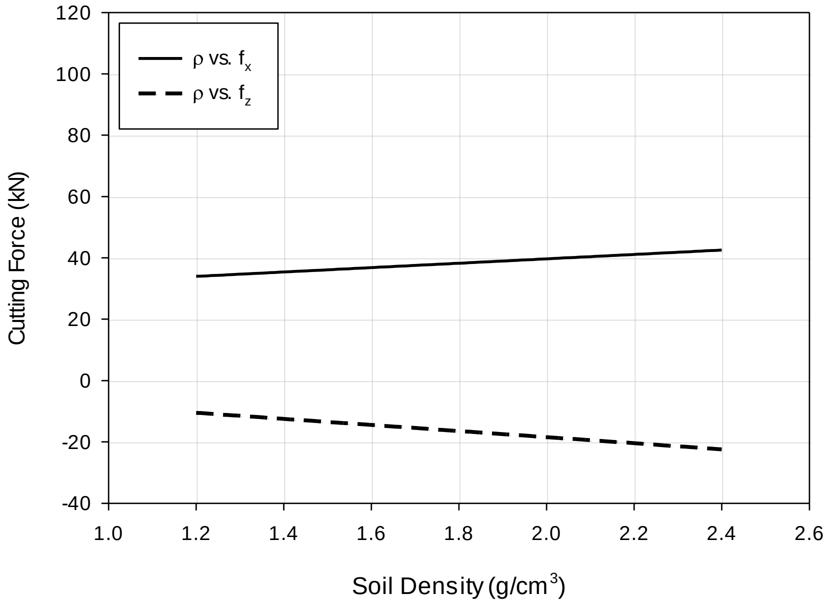

Figure 4.15. Simulated resistive forces for different soil densities

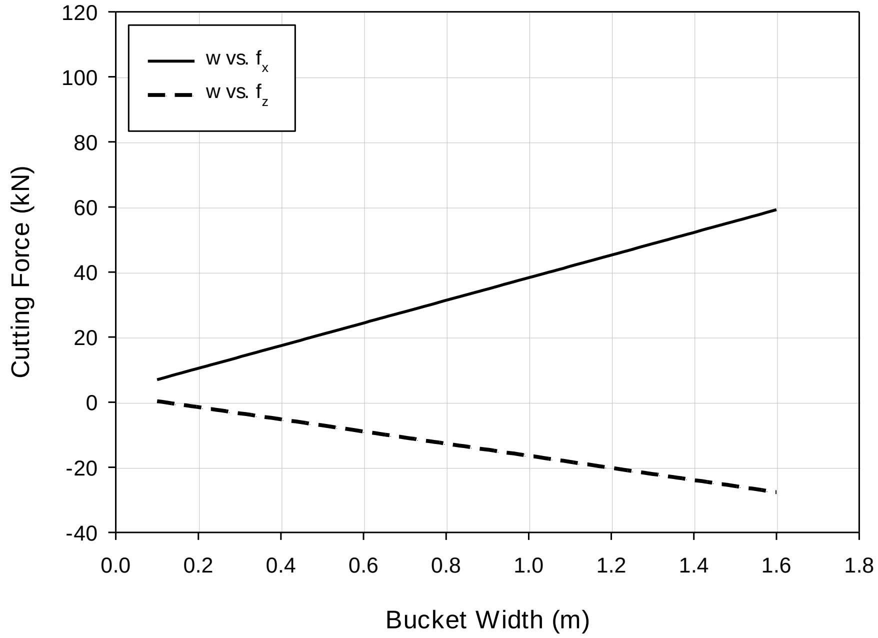

Figure 4.16. Simulated resistive forces for different bucket widths

It is important to highlight some points on the simulation results. For example; when cutting depth is doubled, draft force is not doubled, it becomes approximately four times higher and the relationship is not linear when cutting depth is below 0.8m (Figure 4.12). As another example; when bucket width is doubled, the draft force becomes less than twice of the initial (Figure 4.16). It is also interesting that cohesion increase results in a high increase on horizontal force component, while vertical force component value stays almost same (Figure 4.14).

4.3. Validation Studies

To validate the performance of the simulation developed in this study, comparisons with data obtained from a field experiment, the soil-bin experiments, the results of finite element simulations, discrete element simulations, and finally the results from as a classical method, widely accepted fundamental earth-moving equation model (FEE), were conducted. As Figure 4.17 shows, the new results of this simulation are compared with the four primary soil-tool interaction investigation methods.

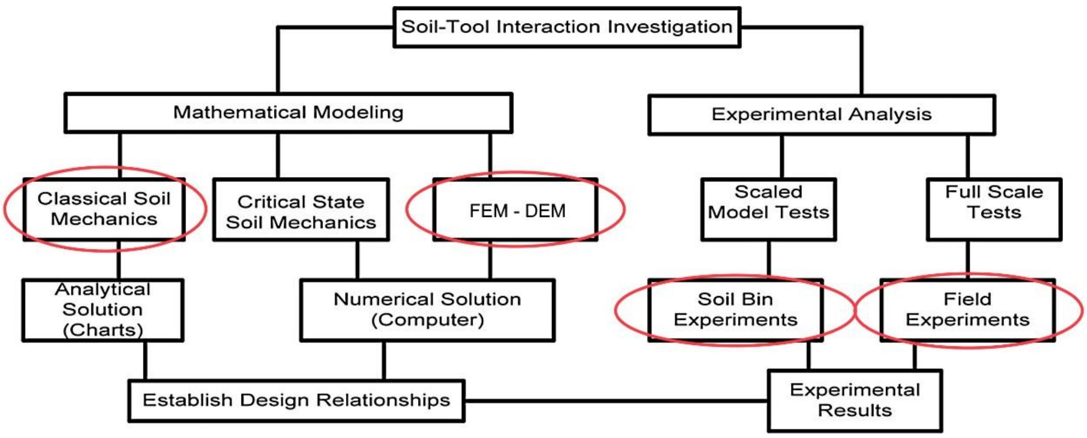

Figure 4.17. Soil-tool investigation methods (Ani et al. 2018).

4.3.1. Comparison with Field Experiment Data

Obermayr et al. (2013) performed an experimental site study on examining the reaction force of cohesionless soils during real excavation. Figure 4.18 shows the experimental setup. A circular trajectory followed by the bucket with the rotation of the arm. During the excavation process, forces generated in hydraulic cylinders were measured and converted to bucket forces. The same soil profile was generated, and the simulation followed the same excavation trajectory Table 4.1. Results can be seen in Figure 4.19 and Figure 4.20.

Table 4.1. *Simulated trajectory and soil properties imported from the field experiment*

$\alpha(°)$	$d(m)$	$\phi(°)$	$\gamma(kN/m^3)$	$c(kPa)$	*Soil Type*	*Condition*
30	0.5	44.8	16.5	0.5	poorly graded gravel with silt	dry

α = Rake Angle, d = Cutting Depth, ϕ = Friction Angle, γ = Unit Weight, c = Cohesion

It is observed that they follow almost similar trends during an excavation for both soil tool model and the experimental data, although there are some differences. Besides, these differences are attributed to both experimental data's precision and the soil properties used in the experiments as they used a soil which was not well defined in terms of engineering properties.

Figure 4.18. Experimental setup (Obermayr et al., 2013)

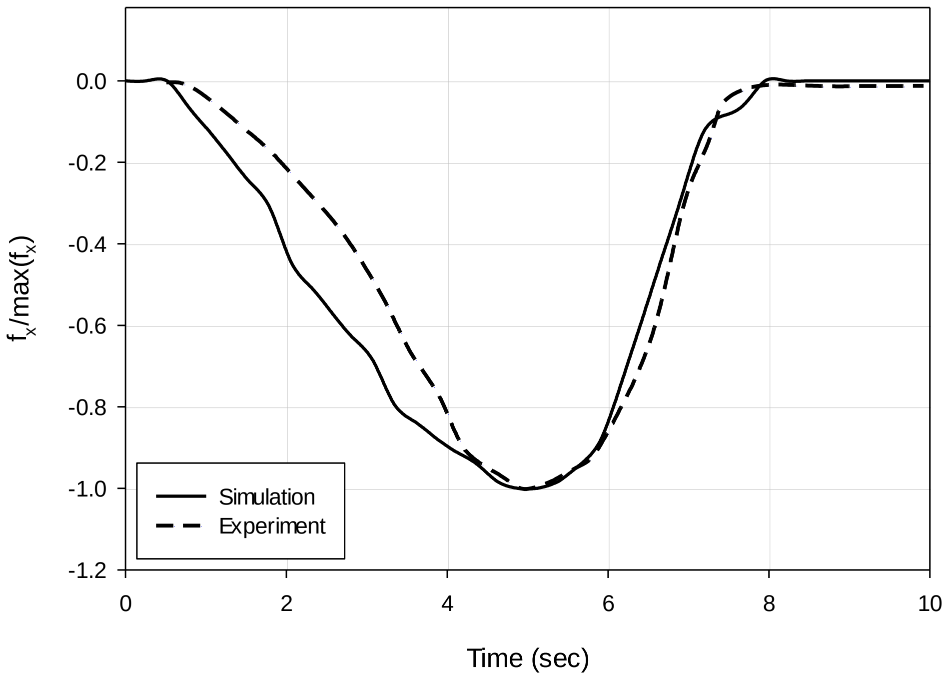

Figure 4.19. Normalized horizontal reaction force (f_x) comparison between experimental and simulation data

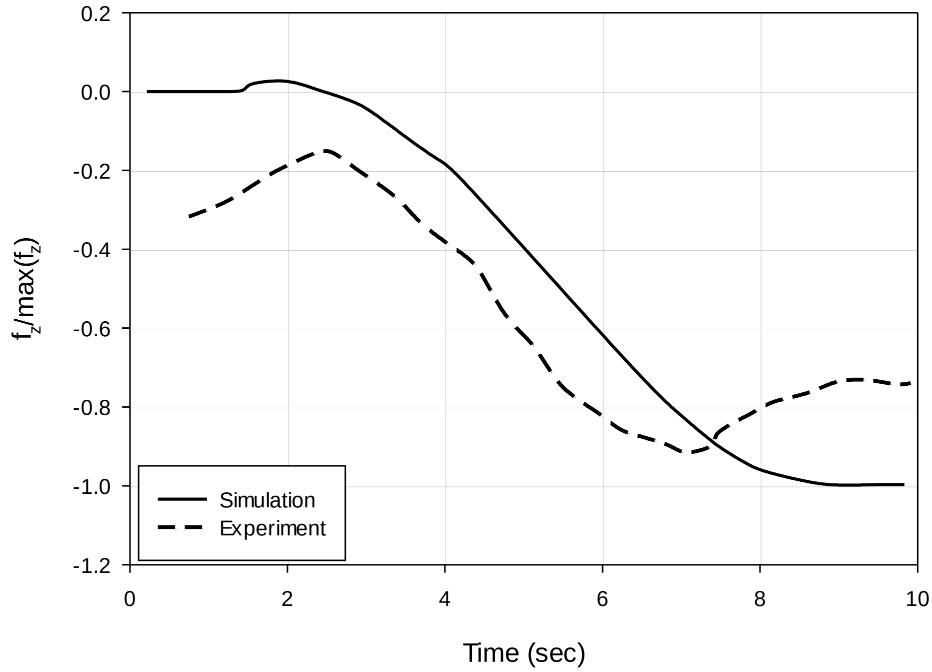

Figure 4.20. Normalized vertical reaction force (f_z) comparison between experimental and simulation data

4.3.2. Comparison with Soil Bin Experiment Data

Soil bin experimental setup is used for obtaining the resistive force of the soil against tillage tools, excavator bucket, and cutting blade. Researchers used these data to understand and verify the accuracy of the data obtained using finite and discrete element methods or classical methods like FEE (Ani et al., 2018). In the literature, Boccafogli et al. (1992) established a soil bin facility to verify the classical wedge model; Qinsen and Shuren (1994) used a soil bin and bulldozer blade to verify their analytical model; Tagar et al. (2014) conducted an experimental soil bin setup to observe resistance force on tillage tool inside a soil with three consistency limits (sticky, plastic and liquid) and Xi et al. (2019) used soil bin test to compare classical methods' results with experimental data on lunar surface where gravity is 1/6 of the gravity on the earth.

Qinsen & Shuren (1994) used a soil-bin test apparatus to obtain experimental data where setup can be seen in Figure 4.21. The dimensions of the soil bin are 30m x 1.2m x 1.0m. A specific type of sandy clay (‘Loess’, from northwestern China) has been used Table 4.2. Cutting process has only the sweeping phase for this experiment.

Table 4.2. *Simulated trajectory and soil properties imported from the soil-bin experiment*

$\alpha(°)$	$d(m)$	$\phi(°)$	$\gamma(kN/m^3)$	$c(kPa)$	*Soil Type*	*Condition*
45	0.03	28	16	20	loess (silt-sized sediment)	dry

α = Rake Angle, d = Cutting Depth, ϕ = Friction Angle, γ = Unit Weight, c = Cohesion

Figure 4.22 reveals that testing with a cutting depth of 30mm and specific gravity of 1.85g/cm^3 shows that the maximum predicted draft force is almost the same with the experimental data. The simulation’s output shows a good agreement with the experimental data.

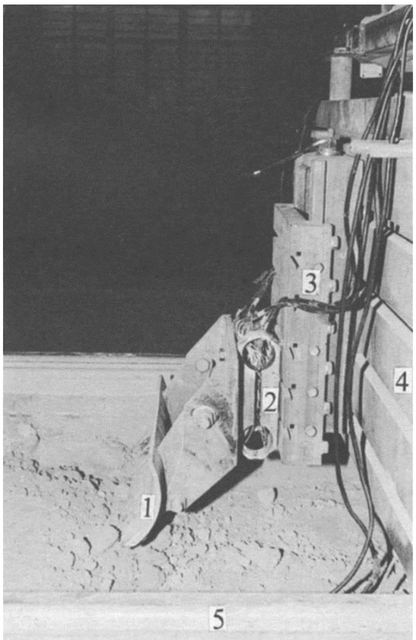

Figure 4.21. Experimental setup: 1, cutting blade; 2, octagonal ring dynamometer; 3, height adjustment apparatus for blade; 4, vehicle pushing the blade forward; 5, soil bin (Qinsen & Shuren, 1994)

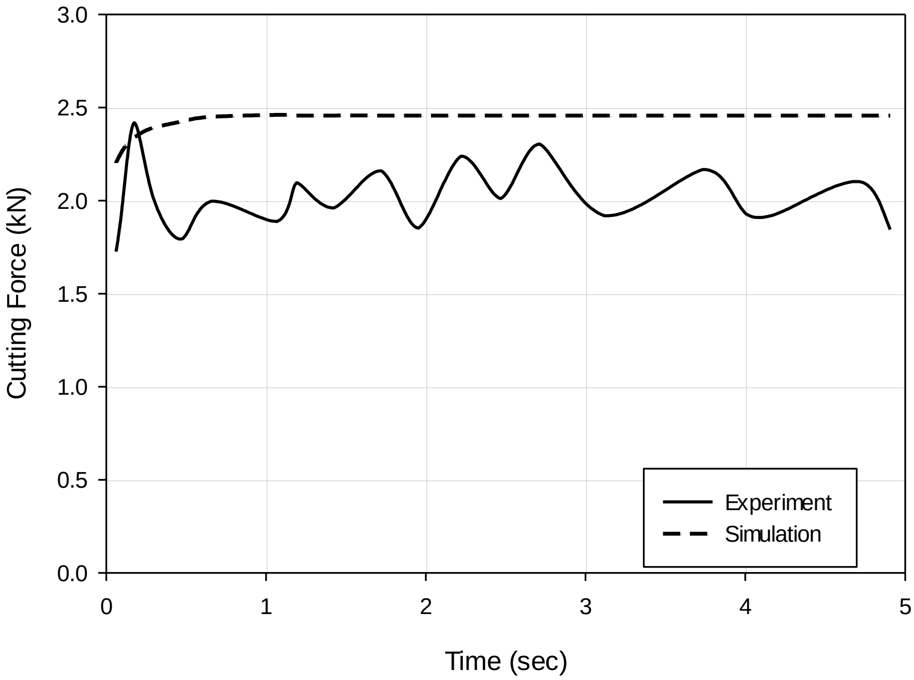

Figure 4.22. Comparison between soil-bin experiment and simulation data

4.3.3. Comparison with FEM

As a secure and relatively new numerical method, the finite element method is also used by researchers dealing with soil-tool interaction subject (Abo-Elnor et al., 2003; Mouazen & Neményi, 1999; Rosa & Wulfsohn, 1999). With a good FEM model, it is possible to investigate the process and observe parameters affecting the draft force.

Abo-Elnor et al. (2004) shared the results of their studies with FEM based soil-tool interaction. They modeled an environment consist of sandy soil with γ = 16 kN/m^3 and ϕ =30° as shown in Figure 4.23. A 600mm width cutting blade has been used to cut soil plane for 50mm. Simulation has been run on the sweeping phase only where there is no digging and loading phases.

Table 4.3. *Simulated trajectory and soil properties imported from the FEM model*

α(°)	*d(m)*	*ϕ(°)*	*γ(kN/m³)*	*c(kPa)*	*Soil Type*	*Condition*
75	0.2	30	16	0.1	karlsruhe sand	dry

α = Rake Angle, d = Cutting Depth, ϕ = Friction Angle, γ = Unit Weight, c = Cohesion

Figure 4.24 shows vertical force outputs during the cutting process for both the FEM model and simulation are very close to each other.

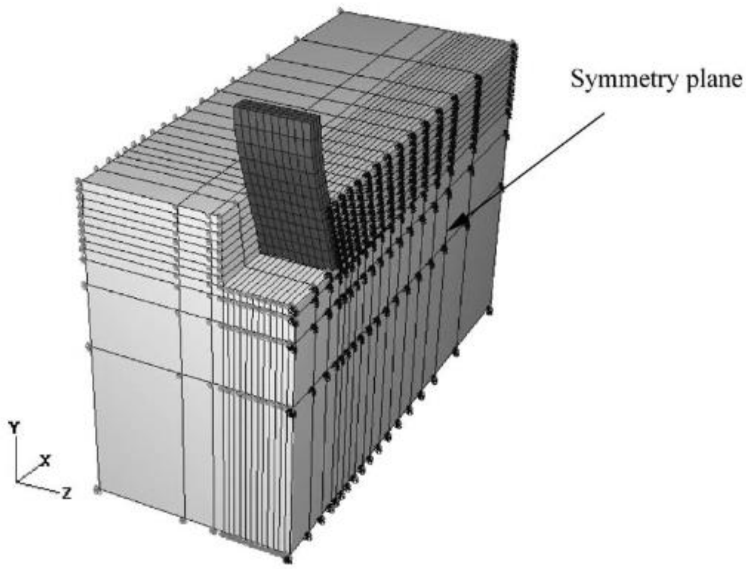

Figure 4.23. FEM model prepared by Abo-Elnor et al. (2004)

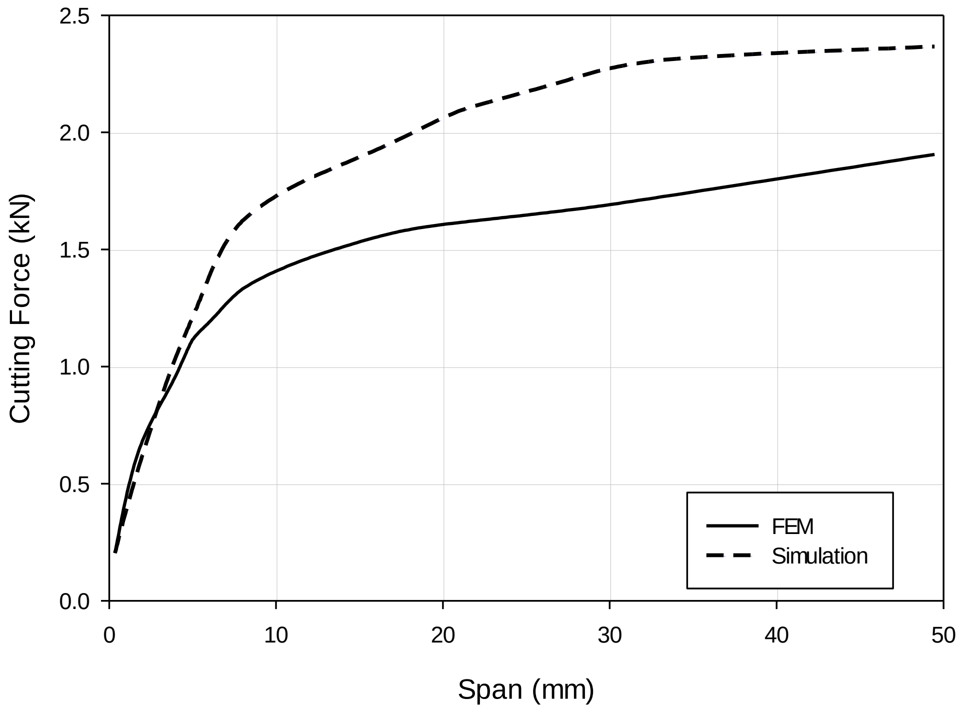

Figure 4.24. Comparison of vertical forces during excavation with simulation data and FEM-based data

4.3.4. Comparison with DEM

As the computer power increased during the last decade, DEM simulations (Jiang et al., 2017; Mak et al., 2012; Obermayr et al., 2011; Coetzee and Els, 2009; Shmulevich et al., 2007; Gaurav, 2008) gained popularity on analyzing complex interactions such as excavation and performed successfully. However, it is hard to construct a DEM model, and it can take too long to analyze a short period. It performs particle-based analysis, and when tiny particle like those of the soil is the case, it requires more computer power and time.

Franco et al. (2007) performed a DEM analysis with a cohesionless soil domain. Unit weight was selected as 17 kN/m^3. Same procedures have been applied with the simulation developed within this study, and the results are listed in the following table. For the reason that the simulation proposed in this thesis has some fundamental assumptions which may not be realistic for very shallow depths (<0.5m) due to varying soil properties and behavior, difference level with the DEM results came up high as can be seen in Table 4.4. Still, DEM is extremely time consuming compared with the soil tool model developed in this study.

Table 4.4. *Comparison of reaction forces with different cases for the DEM analysis and the simulation*

α(°)	ϕ(°)	d(m)	F_{zDEM}(kN)	F_{zSIM}(kN)	F_{xDEM}(kN)	F_{xSIM}(kN)	Difference F_z(%)	Difference F_x(%)
72	14	0.15	0.36	0.37	1.23	1.02	2.9	-20.9
72	18	0.15	0.45	0.44	1.47	0.80	-1.2	-82.9
72	25	0.15	0.4	0.37	1.32	1.06	-7.9	-24.8
72	31	0.15	0.55	0.29	1.76	1.25	-87.9	-40.4
72	35	0.15	0.42	0.23	2.13	1.55	-80.2	-37.2
72	18	0.1	0.17	0.14	0.63	0.46	-19.1	-38.4
72	18	0.2	0.82	0.64	2.57	1.32	-27.7	-95.3
45	18	0.15	1.07	1.05	1.17	0.67	-1.7	-73.5
63	18	0.15	0.65	0.62	1.3	0.90	-4.3	-44.1
90	18	0.15	-0.03	-0.04	1.73	1.39	17.3	-24.8

α = Rake Angle, ϕ = Friction Angle, d = Cutting Depth, F_{zDEM} = Vertical Cutting Force in DEM, F_{zSIM} = Vertical Cutting Force in Simulation, F_{xDEM} = Horizontal Cutting Force in DEM, F_{xSIM} = Horizontal Cutting Force in Simulation

4.3.5. Comparison with FEE

Ni et al. (2013) stated that when the excavation depth was increased, the digging force also increases gradually. To reveal this fact, the results of a simulation with a widely accepted Fundamental Earth-Moving Equation (FEE) model was represented.

Table 4.5. *Simulated trajectory and soil properties imported from the FEE model for horizontal force comparison*

$\alpha(°)$	$d(m)$	$\phi(°)$	$\gamma(kN/m^3)$	$c(kPa)$	*Soil Type*	*Condition*
80	0.6	24	20	15	very stiff clay	dry
80	0.8	24	20	15	very stiff clay	dry
80	1.1	24	20	15	very stiff clay	dry

Figure 4.25 shows the trajectories of three digging operations which were performed with different digging depths and different spans. Comparison of bucket forces calculated from the FEE model and the simulation is displayed in Figure 4.26. As can be seen, there is a good agreement between these two data sets.

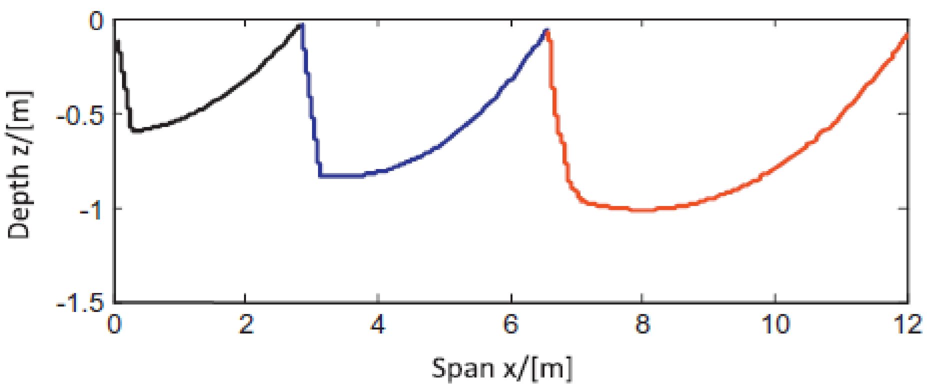

Figure 4.25. Trajectories of bucket tip (Ni et al., 2013)

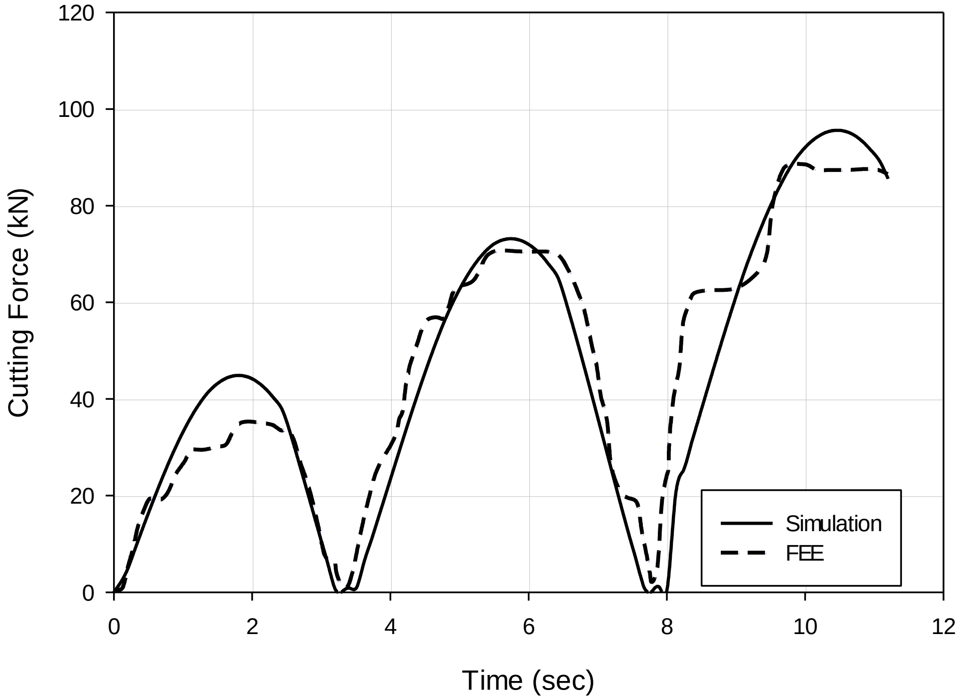

Figure 4.26. Comparison of reaction on cohesive-stiff soil with the same trajectories between extended FEE model and the simulation developed in this study

Another study with Fundamental Earth-Moving Equation (FEE) was conducted by Patel and Prajapati (2012). Changes in total resistive force with the same trajectory and different soil friction angle has been displayed. Applying the same procedure in the method represented in this study, almost the same results were obtained (Figure 4.27).

Table 4.6. *Simulated trajectory and soil properties imported from the FEE model for comparison of force change with the soil friction angle*

α(°)	*d(m)*	*ϕ(°)*	*γ(kN/m³)*	*c(kPa)*	*Soil Type*	*Condition*
45	0.3	44	28	25	hard clay	dry

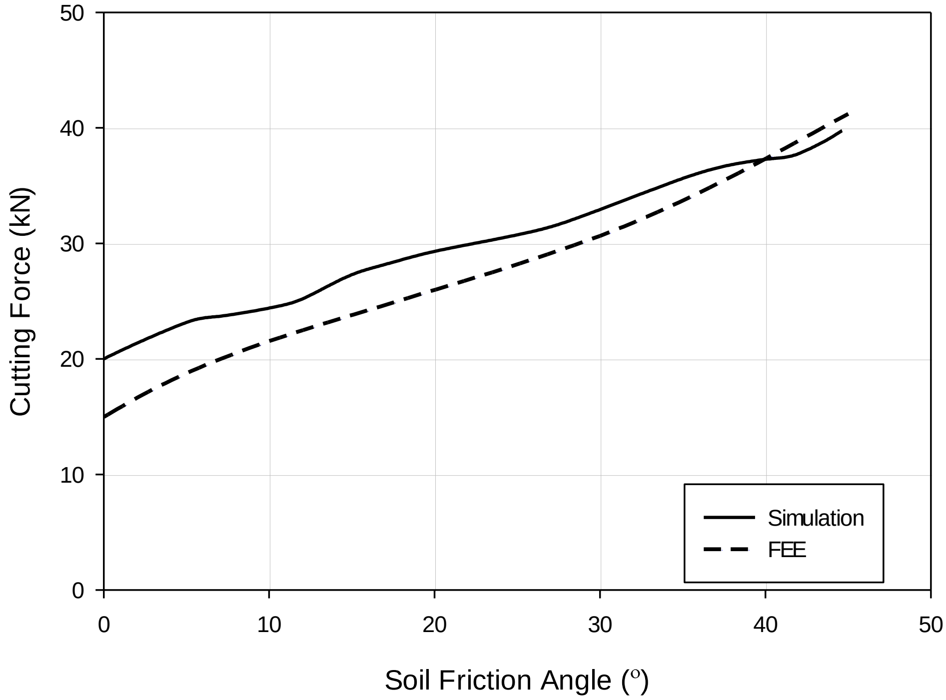

Figure 4.27. Comparison of total horizontal force (Fx) change in different soil friction angle between FEE model and the method represented in this study

Results show that the new method developed in this study can be an excellent alternative to predict resistive forces generated during the excavation process. There are some minor differences with experimental data, which is tolerable considering the field applications where a high accuracy may not be achieved due to variations in soil material properties. As the problem is very complex, a computationally inexpensive model with a reasonable accuracy can be accepted.

CHAPTER 5

SUMMARY, CONCLUSIONS AND FUTURE WORKS

5.1. Summary

Excavation is one of the main demanding tasks in construction fields. To handle this requirement, a vast number of excavators are operating around the globe. Researchers and companies put a lot of efforts to develop more efficient excavator models. With the advancement of technology, autonomous systems become a trendy and ideal way to upgrade machines for better efficiencies. Not surprisingly, there have been considerably many attempts to develop a fully autonomous excavation system. Unfortunately, these attempts did not conclude well as there are no fully autonomous excavators working on sites yet. Considering underlying reasons, some key challenges appear, one of them being the reliable estimation for soil-tool interaction behavior. The complexity of the problem makes it harder to generate an accurate model considering all the variables affecting the excavation operation. Current solutions are generally computationally expensive, which is not suitable for real-time applications. Moreover, the offered models do not cover the whole excavation phases (digging, sweeping, loading, and unloading).

In this research, a new method has been developed to have an accurate prediction for soil-tool reaction forces, real-time solution for the visualization process, and excavator-soil model which covers whole excavation phases. A computer program has been written in MATLAB environment, which can be used to gather information including the soil properties and display forces generated during an excavation in real-time. The excavator simulator models the excavations for various types of soils including sands and clays with varying relative densities and consistencies, respectively.

5.2. Conclusions

The simulation studies are made through the graphical user interface. The calculated responses are observed through graphical user interface in addition to the visual outputs. The validation studies are done using five different resources available in the literature, which are namely the field experiment data, Soil Bin experiment data, the data obtained through finite element methods and discrete element methods, and outcomes obtained through fundamental earth moving equation. The following conclusions are drawn when the results obtained are investigated in detail:

- The major advantage of the proposed method is its time relaxation during the excavation process when compared to other proposed solutions. This can be thought as a very good achievement as the current trend in such simulation tools is to have a very quick response, i.e., almost real time, with a reasonable accuracy.
- Comparison with the field data showed that the excavation tool simulation developed in this study follows almost similar trends with the experimental data. Although there are some differences in terms of magnitudes of the forces they are attributed to soil properties used in the experiments.
- Comparison with the soil bin experiment shows a good agreement with the experimental data, which is a practically significant achievement.
- The outputs of the finite element method in terms of vertical force during the cutting process are very close to ones obtained through the soil tool model.
- The discrete element method outputs are somewhat different from the ones developed in this thesis. The reasons may be that the assumptions of the soil tool model may not be realistic for very shallow depths (<0.5m) due to varying soil properties and behavior, which needs to be investigated in the further studies.
- Finally, comparison of bucket forces calculated from the Fundamental Earth Moving Equation model shows that there is a very good agreement between these two models.

In short, results of the simulation studies show that the new method presented in this research have a good agreement with experimental and other widely accepted force calculation models' data. However, when the cutting depth is so small (< 0.2m) or bucket width is small (< 0.1m), the algorithm gives conservative responses which are not close to experimental results. Considering these, the effects of dynamic forces including the impact forces, the effects due to water may be improved. Some improvements are planned on algorithms to overcome this situation in future studies.

5.3. Future Work

Considering the need for automated machines to be used in construction fields, there are many research studies that can be performed as a follow up for this work. An incomplete list of them are itemized below:

- In addition to automated excavation systems, this new method can be used to develop efficient operator training simulations, computer games, and virtual reality-based simulations. In the future study, the authors will attack soil-tool interaction in 3-D scale with an accurate prediction of resistive forces and visual deformations in the excavated region.
- Besides, in the future phases of the simulation studies, the software needs to be able to predict the phase of the bucket, i.e., digging, sweeping, loading, unloading, according to surface orientation, bucket orientation, velocity, moving direction. Active force combination needs to be arranged automatically with the current phase.
- When the surficial soils are considered, effects of unsaturated medium, especially in dynamic nature, can be embedded to the software to more accurately capture the field behavior.
- The material library considered in this study can further be enhanced considering various types of soils especially cobbles, boulders, etc.

considering the fact that excavator companies are currently focusing more efficient models to be used in fields comprising of such soils.

- The geometry of different buckets should be embedded to the software to cover wide range of excavators used available in the construction market.
- The response of the excavator operator also needs to be considered when designing the software, therefore developed GUI should be modified based on the UX-User Experience.
- Comparison of the results with developed software and the field data can be enhanced through the sensors embedded into the excavators bucket to measure the field response during excavation.

REFERENCES

Abo-Elnor, M., Hamilton, R., & Boyle, J. . (2003). 3D Dynamic Analysis of Soil–tool Interaction Using the Finite Element Method. *Journal of Terramechanics*, *40*(1), 51–62. https://doi.org/10.1016/j.jterra.2003.09.002

Abo-Elnor, M., Hamilton, R., & Boyle, J. . (2004). Simulation of Soil–blade Interaction for Sandy Soil Using Advanced 3D Finite Element Analysis. *Soil and Tillage Research*, *75*(1), 61–73. https://doi.org/10.1016/S0167-1987(03)00156-9

Ani, O. A., Uzoejinwa, B. B., Ezeama, A. O., Onwualu, A. P., Ugwu, S. N., & Ohagwu, C. J. (2018). Overview of soil-machine interaction studies in soil bins. *Soil and Tillage Research*, *175*(September 2016), 13–27. https://doi.org/10.1016/j.still.2017.08.002

Bishop, A. W., Alpan, I., Blight, G. E., & Donald, I. B. (1960). Factors Controlling the Strength of Partly Saturated Cohesive Soils. *Proc. Am. Sot. Ciu. Engrs Research Conj: Shear Strength of Cohesive Soils*, 503–532.

Blouin, S., Hemami, A., & Lipsett, M. (2001). Review of Resistive Force Models for Earthmoving Processes. *Journal of Aerospace Engineering*, *14*(3), 102–111. https://doi.org/10.1061/(ASCE)0893-1321(2001)14:3(102)

Boccafogli, A., Busatti, G., Gherardi, F., Malaguti, F., & Paoluzzi, R. (1992). Experimental Evaluation of Cutting Dynamic Models in Soil Bin Facility. *Journal of Terramechanics*, *29*(1), 95–105. https://doi.org/10.1016/0022-4898(92)90017-E

Bodson, M. (2003). Fun Control Experiments with Matlab and a Joystick. *42nd IEEE International Conference on Decision and Control (IEEE Cat. No.03CH37475)*, *3*, 2508–2513. https://doi.org/10.1109/CDC.2003.1272998

Boles, W. W., Scott, W. D., & Connolly, J. F. (1997). Excavation Forces in Reduced Gravity Environment. *Journal of Aerospace Engineering*, *10*(2), 99–103. https://doi.org/10.1061/(ASCE)0893-1321(1997)10:2(99)

Bonitz, R., Shiraishi, L., Robinson, M., Carsten, J., Volpe, R., Trebi-Ollennu, A., … Davis, K. R. (2009). The Phoenix Mars Lander Robotic Arm. *2009 IEEE Aerospace Conference*, (December 2013), 1–12. https://doi.org/10.1109/AERO.2009.4839306

Buildsum. (2014). Angle of Repose. Retrieved March 7, 2019, from http://buildsum.blogspot.com/2014/06/angle-of-repose-zone-of-influence.html

Cannon, H. N. (1999). *Extended Earthmoving with an Autonomous Excavator*. Carnegie Mellon University.

Coetzee, C. J., & Els, D. N. J. (2009). The Numerical Modelling of Excavator Bucket Filling using DEM. *Journal of Terramechanics*, *46*(5), 217–227. https://doi.org/10.1016/j.jterra.2009.05.003

Coleman, J. D. (1962). Stress-Strain Relations for Partially Saturated Soils. *Geotechnique*, *12*(4), 348–350.

Coulomb, C. (1776). *Essai Sur une Application des Règles de Maximis & Minimis à Quelques Problèmes de Statique, Relatifs à L'architecture*.

Dadhich, S., Bodin, U., & Andersson, U. (2016). Key Challenges in Automation of Earth-moving Machines. *Automation in Construction*, *68*, 212–222. https://doi.org/10.1016/j.autcon.2016.05.009

Dukkipati, R. V. (2010). MATLAB An Introduction with Applications. In *New Age International* (Vol. 1). https://doi.org/10.1017/CBO9781107415324.004

Escario, V., & Sáez, J. (1986). The Shear Strength of Partly Saturated Soils. *Géotechnique*, *36*(3), 453–456. https://doi.org/10.1680/geot.1986.36.3.453

Fredlund, D. G., & Rahardjo, H. (1993). Soil Mechanics for Unsaturated Soils. In *John Wiley & Sons, Inc.* (Vol. 30). https://doi.org/10.1002/9780470172759

Fredlund, D G, Morgenstern, N. R., & Widger, R. a. (1978). The Shear Strength of Unsaturated Soils. *Canadian Geotechnical Journal*, *15*(3), 313–321. https://doi.org/10.1139/t78-029

Fredlund, Delwyn G., Rahardjo, H., & Gan, J. K. M. (1989). Non-linearity of Strength Envelope for Unsaturated Soils. *International Journal of Rock Mechanics and Mining Sciences & Geomechanics Abstracts*, *26*(1), A8. https://doi.org/10.1016/0148-9062(89)90592-5

Gaurav, M. (2008). *Design and Development of an Excavator Attachment*. Nirma University.

Ghazavi, M., Hosseini, M., & Mollanouri, M. (2008). A Comparison Between Angle of Repose and Friction Angle of Sand. *International Association for Computer Methods and Advances in Geomechanics*, 1272–1275. Retrieved from http://scholar.google.com/scholar?hl=en&btnG=Search&q=intitle:A+Comparison+between+Angle+of+Repose+and+Friction+Angle+of+Sand#0

Gill, W. R., & Vandenberg, G. . (1968). Soil Dynamics in Tillage and Traction. *Journal of Terramechanics*, *5*(4), 65–66. https://doi.org/10.1016/0022-4898(68)90055-4

Godwin, R. J., & O'Dogherty, M. J. (2007). Integrated Soil Tillage Force Prediction Models. *Journal of Terramechanics*, *44*(1), 3–14.

https://doi.org/10.1016/j.jterra.2006.01.001

Head, K. H. (2006). *Manual of Soil Laboratory Testing*. Whittles Publishing.

Hemami, A., Goulet, S., & Aubertin, M. (1994). Resistance of Particulate Media to Excavation: Application to Bucket Loading. *International Journal of Surface Mining, Reclamation and Environment*, *8*(3), 125–129. https://doi.org/10.1080/09208119408964772

Hettiaratchi, D. R. P., Witney, B. D., & Reece, A. R. (1966). The Calculation of Passive Pressure in Two-dimensional Soil Failure. *Journal of Agricultural Engineering Research*, *11*(2), 89–107. https://doi.org/10.1016/S0021-8634(66)80045-8

Hidromek A.Ş. (2017). Hidromek HMK300LC Ekskavatör Katalog. Retrieved May 18, 2017, from http://www.hidromek.com.tr/upload/dokumanlar/1252017135312482_300lc_lr_tr_katalog.pdf

Jiang, M., Xi, B., Arroyo, M., & Rodriguez-Dono, A. (2017). DEM Simulation of Soil-tool Interaction Under Extraterrestrial Environmental Effects. *Journal of Terramechanics*, *71*, 1–13. https://doi.org/10.1016/j.jterra.2017.01.002

Khalili, N., & Khabbaz, M. H. (1998). A Unique Relationship for χ for the Determination of the Shear Strength of Unsaturated Soils. *Géotechnique*, *48*(5), 681–687. https://doi.org/10.1680/geot.1998.48.5.681

Kim, Y. B., Ha, J., Kang, H., Kim, P. Y., Park, J., & Park, F. C. (2013). Dynamically Optimal Trajectories for Earthmoving Excavators. *Automation in Construction*, *35*, 568–578. https://doi.org/10.1016/j.autcon.2013.01.007

Knappett, J. A., & Craig, R. F. (2012). *Craig's Soil Mechanics* (Eighth).

Leite, E. P. (2010). *Matlab - Modelling, Programming and Simulations* (E. Pereira, Ed.). https://doi.org/10.5772/242

Li, J., Li, L., Sun, D., & Rao, P. (2016). Analysis of Undrained Cylindrical Cavity Expansion Considering Three-Dimensional Strength of Soils. *International Journal of Geomechanics*, *16*(5), 04016017. https://doi.org/10.1061/(ASCE)GM.1943-5622.0000650

Maciejewski, J., Jarzębowski, A., & Trąmpczyński, W. (2003). Study on the Efficiency of the Digging Process Using the Model of Excavator Bucket. *Journal of Terramechanics*, *40*(4), 221–233. https://doi.org/10.1016/j.jterra.2003.12.003

Mak, J., Chen, Y., & Sadek, M. A. (2012). Determining Parameters of a Discrete Element Model for Soil–tool Interaction. *Soil and Tillage Research*, *118*, 117–122. https://doi.org/10.1016/j.still.2011.10.019

Mayne, P. W., Schneider, J. A., Yu, H. S., & Mitchell, J. K. (1999). Analysis of Cone Resistance: Review of Methods. *Journal of Geotechnical and Geoenvironmental Engineering*, *125*(9), 812–814. https://doi.org/10.1061/(ASCE)1090-0241(1999)125:9(812)

McKyes, E. (1985). Soil Cutting and Tillage. In *Developments in Agricultural Engineering* (pp. 1–217).

Mouazen, A. M., & Neményi, M. (1999). Finite Element Analysis of Subsoiler Cutting in Non-homogeneous Sandy Loam Soil. *Soil and Tillage Research*, *51*(1–2), 1–15. https://doi.org/10.1016/S0167-1987(99)00015-X

Ni, T., Zhang, H., Yu, C., Zhao, D., & Liu, S. (2013). Design of Highly Realistic Virtual Environment for Excavator Simulator. *Computers & Electrical Engineering*, *39*(7), 2112–2123. https://doi.org/10.1016/j.compeleceng.2013.06.010

Obermayr, M., Dressler, K., Vrettos, C., & Eberhard, P. (2011). Prediction of Draft Forces in Cohesionless Soil with the Discrete Element Method. *Journal of Terramechanics*, *48*(5), 347–358. https://doi.org/10.1016/j.jterra.2011.08.003

Obermayr, M., Vrettos, C., Kleinert, J., & Eberhard, P. (2013). A Discrete Element Method for Assessing Reaction Forces in Excavation Tools. *Congreso de Métodos Numéricos En Ingeniería*, 1–17. Retrieved from http://www.researchgate.net/publication/236870184_a_discrete_element_method_for_assessing_reaction_forces_in_excavation_tools/file/9c960519bd1ce48164.pdf

Onwualu, A. (1998). Draught and Vertical Forces Obtained from Dynamic Soil Cutting by Plane Tillage Tools. *Soil and Tillage Research*, *48*(4), 239–253. https://doi.org/10.1016/S0167-1987(98)00127-5

Park, B. (2002). *Development of a Virtual Reality Excavator Simulator: a Mathematical Model of Excavator Digging and a Calculation Methodology*.

Patel, B. P., & Prajapati, J. M. (2012). Evaluation of Resistive Force using Principle of Soil Mechanics for Mini Hydraulic Backhoe Excavator. *International Journal of Machine Learning and Computing*, *2*(4), 386–391. https://doi.org/10.7763/IJMLC.2012.V2.150

Pufahl, D. E., Fredlund, D. G., & Rahardjo, H. (1983). Lateral Earth Pressures in Expansive Clay Soils. *Canadian Geotechnical Journal*, *20*(2), 228–241. https://doi.org/10.1139/t83-027

Qinsen, Y., & Shuren, S. (1994). A Soil-tool Interaction Model for Bulldozer Blades. *Journal of Terramechanics*, *31*(2), 55–65. https://doi.org/10.1016/0022-4898(94)90007-8

Rankine, W. J. M. (1891). *A Manual of Civil Engineering*.

Reece, A. R. (1964). The Fundamental Equation of Earth-Moving Mechanics. *Proceedings of the Institution of Mechanical Engineers, Conference Proceedings*, *179*(6), 16–22. https://doi.org/10.1243/PIME_CONF_1964_179_134_02

Rosa, U. A., & Wulfsohn, D. (1999). Constitutive Model for High Speed Tillage Using Narrow Tools. *Journal of Terramechanics, 36*(4), 221–234. https://doi.org/10.1016/S0022-4898(99)00006-3

Russell, A. R., & Khalili, N. (2006). Cavity Expansion Theory and the Cone Penetration Test in Unsaturated Sands. *Unsaturated Soils 2006*, 2546–2557. https://doi.org/10.1061/40802(189)217

Russell, A.R. (2004). *Cavity Expansion in Unsaturated Soils*. University of New South Wales Sydney.

Russell, Adrian R., & Khalili, N. (2006). On the Problem of Cavity Expansion in Unsaturated Soils. *Computational Mechanics*, *37*(4), 311–330. https://doi.org/10.1007/s00466-005-0672-7

SAE International. (1999). *SAE J296 - Mini excavator and backhoe bucket volumetric rating*.

Shazali. Osman, M. (1969). The Mechanics of Soil Cutting Blades. *J. Agric. Engineering Res*, *9*.

Shmulevich, I., Asaf, Z., & Rubinstein, D. (2007). Interaction Between Soil and a Wide Cutting Blade Using the Discrete Element Method. *Soil and Tillage Research*, *97*(1), 37–50. https://doi.org/10.1016/j.still.2007.08.009

Singh, S. (1995). Learning to Predict Resistive Forces During Robotic Excavation. *Proceedings of 1995 IEEE International Conference on Robotics and Automation*, *2*, 2102–2107. https://doi.org/10.1109/ROBOT.1995.526025

Singh, S. (1997). State of the Art in Automation of Earthmoving. *Journal of Aerospace Engineering*, *10*(4), 179–188. https://doi.org/10.1061/(ASCE)0893-1321(1997)10:4(179)

Skonieczny, K. (2018). Modeling the Effects of Surcharge Accumulation on Terrestrial and Planetary Wide-blade Soil–tillage Tool Interactions. *Soil and Tillage Research*, *176*(March 2017), 104–111. https://doi.org/10.1016/j.still.2017.11.009

Swick, W. C., & Perumpral, J. V. (1988). A Model for Predicting Soil-tool Interaction. *Journal of Terramechanics, 25*(1), 43–56. https://doi.org/10.1016/0022-4898(88)90061-4

Tagar, A. A., Ji, C., Ding, Q., Adamowski, J., Chandio, F. A., & Mari, I. A. (2014). Soil Failure Patterns and Draft as Influenced by Consistency Limits: An

Evaluation of the Remolded Soil Cutting Test. *Soil and Tillage Research*, *137*, 58–66. https://doi.org/10.1016/j.still.2013.12.001

Terzaghi, K. (1943). Theoretical Soil Mechanics. In *John Wiley & Sons, Inc*. https://doi.org/10.1680/geot.1964.14.1.1

Tong, J., Ren, L., Chen, B., & Qaisrani, A. R. (1994). Characteristics of Adhesion between Soil and Solid Surfaces. *Journal of Terramechanics*, *31*(2), 93–105. https://doi.org/10.1016/0022-4898(94)90009-4

Tsuji, T., Nakagawa, Y., Matsumoto, N., Kadono, Y., Takayama, T., & Tanaka, T. (2012). 3-D DEM Simulation of Cohesive Soil-pushing Behavior by Bulldozer Blade. *Journal of Terramechanics*, *49*(1), 37–47. https://doi.org/10.1016/j.jterra.2011.11.003

Vahed, S. M., Song, X., Dai, J. S., Lam, H. K., Seneviratne, L. D., & Althoefer, K. (2008). Soil Estimation Based on Dissipation Energy during Autonomous Excavation. *IFAC Proceedings Volumes*, *41*(2), 13821–13826. https://doi.org/10.3182/20080706-5-KR-1001.02340

Wheeler, P. N., & Godwin, R. J. (1996). Soil Dynamics of Single and Multiple Tines at Speeds up to 20km/h. *Journal of Agricultural Engineering Research*, *63*(3), 243–249. https://doi.org/10.1006/jaer.1996.0026

Wilkinson, A., & DeGennaro, A. (2007). Digging and Pushing Lunar Regolith: Classical Soil Mechanics and the Forces Needed for Excavation and Traction. *Journal of Terramechanics*, *44*(2), 133–152. https://doi.org/10.1016/j.jterra.2006.09.001

William Richardson-Little, & C. J. Damaren. (2005). Position Accommodation and Compliance Control for Robotic Excavation. *Proceedings of 2005 IEEE Conference on Control Applications, 2005. CCA 2005.*, 1194–1199. https://doi.org/10.1109/CCA.2005.1507293

Willman, B. M., & Boles, W. W. (1995). Soil-Tool Interaction Theories as They Apply to Lunar Soil Simulant. *Journal of Aerospace Engineering*, *8*(2), 88–99. https://doi.org/10.1061/(ASCE)0893-1321(1995)8:2(88)

Xi, B., Jiang, M., Cui, L., Liu, J., & Lei, H. (2019a). Experimental verification on analytical models of lunar excavation. *Journal of Terramechanics*, *83*, 1–13. https://doi.org/10.1016/j.jterra.2019.01.002

Xi, B., Jiang, M., Cui, L., Liu, J., & Lei, H. (2019b). Experimental Verification on Analytical Models of Lunar Excavation. *Journal of Terramechanics*, *83*, 1–13. https://doi.org/10.1016/j.jterra.2019.01.002

Y. Franco, D. Rubinstein, & I. Shmulevich. (2007). Prediction of Soil-Bulldozer Blade Interaction Using Discrete Element Method. *Transactions of the ASABE*, *50*(2), 345–353. https://doi.org/10.13031/2013.22625

Zelenin, A. N., Balovnev, V. I., & Kerov, I. P. (1992). *Machines for Moving the Earth*. Rotterdam.

Zhai, Q., & Rahardjo, H. (2012). Determination of Soil–Water Characteristic Curve Variables. *Computers and Geotechnics*, *42*, 37–43. https://doi.org/10.1016/j.compgeo.2011.11.010